NASA TECHNICAL NOTE

NASA TN D-5948

NASA TN D-5948

ANGLE-OF-ATTACK ANALYSIS OF A SPINNING SLENDER CONE WITH SLIGHT AERODYNAMIC AND MASS ASYMMETRIES (REENTRY F)

by Gerard E. Woodbury and W. Douglas Morris

Langley Research Center
Hampton, Va. 23365

NATIONAL AERONAUTICS AND SPACE ADMINISTRATION • WASHINGTON, D. C. • SEPTEMBER 1970

1. Report No.	2. Government Accession No.	3. Recipient's Catalog No.
NASA TN D-5948		

4. Title and Subtitle
ANGLE-OF-ATTACK ANALYSIS OF A SPINNING SLENDER CONE WITH SLIGHT AERODYNAMIC AND MASS ASYMMETRIES (REENTRY F)

5. Report Date: September 1970

6. Performing Organization Code:

7. Author(s)
Gerard E. Woodbury and W. Douglas Morris

8. Performing Organization Report No.: L-7215

9. Performing Organization Name and Address
NASA Langley Research Center
Hampton, Va. 23365

10. Work Unit No.: 124-07-23-10

11. Contract or Grant No.:

12. Sponsoring Agency Name and Address
National Aeronautics and Space Administration
Washington, D.C. 20546

13. Type of Report and Period Covered: Technical Note

14. Sponsoring Agency Code:

15. Supplementary Notes

16. Abstract

An analysis of the flight motions of the Reentry F spacecraft was made by using a combination of a force method and an application of the angular-rate solution of the linearized equations of motion since a trim buildup due to flight-induced asymmetries introduced an error into the ordinarily determined angle of attack. The analysis revealed that the spacecraft had little or no asymmetries prior to and during pitch-roll resonance. However, as the spacecraft emerged from resonance, a slight trim angle of attack was noted which shortly thereafter experienced a reversal in orientation and a subsequent rapid growth in the same general direction to a maximum of 0.87^{o}.

17. Key Words (Suggested by Author(s))	18. Distribution Statement
Angle of attack Slender asymmetric cone Hypersonic reentry	Unclassified – Unlimited

19. Security Classif. (of this report)	20. Security Classif. (of this page)	21. No. of Pages	22. Price*
Unclassified	Unclassified	37	$3.00

*For sale by the Clearinghouse for Federal Scientific and Technical Information
Springfield, Virginia 22151

ANGLE-OF-ATTACK ANALYSIS OF A SPINNING SLENDER CONE WITH SLIGHT AERODYNAMIC AND MASS ASYMMETRIES (REENTRY F)

By Gerard E. Woodbury and W. Douglas Morris
Langley Research Center

SUMMARY

An investigation of the flight motions of the Reentry F spacecraft was made with a combination of a force method and an application of the angular-rate solution of the linearized equations of motion. This type of analysis was necessary because a trim angle-of-attack buildup due to flight-induced asymmetries introduced an error in the ordinarily determined angle of attack in the form of a bias. This bias is the angular displacement of the zero normal-force coefficient from the origin which occurs when trim-producing asymmetries are present. This bias is usually small and normally has been neglected in most previous work. However, since the maximum angle of attack of the Reentry F spacecraft was on the order of 1°, this error could not be ignored.

The results of the analysis showed that the spacecraft had little or no asymmetries prior to and during pitch-roll resonance. However, immediately after resonance, a slight trim angle of attack was noted which shortly thereafter experienced a reversal in orientation and a subsequent rapid growth in the same general direction to a maximum of 0.87°. The spacecraft also experienced a dynamic instability during the same general time period. The effects of either multiple asymmetries or a bent body were also discerned.

INTRODUCTION

The Turbulent Heating Experiment (Reentry F) is a National Aeronautics and Space Administration research flight project to obtain turbulent heat-transfer data and to study boundary-layer transition phenomena under simultaneous conditions of high Mach number, Reynolds number, and total enthalpy. These data are to be used to evaluate existing heat-transfer correlations at the flight conditions of advanced vehicles. In order to do so, it is necessary not only to obtain good quality heating data, but also to define the local environment under which the data are obtained. Since the local environment and the heating rates on a slender body are very sensitive to the orientation of the body with respect to the free stream, the angle-of-attack history of the spacecraft during flight must be determined.

The purpose of this report is to analyze the motions and determine the magnitude and frequencies of the angle of attack of the Reentry F spacecraft during the experiment period.

The flight test was conducted April 27, 1968, from Wallops Station, Virginia. Although the basic objectives of the flight test were achieved, the reentry spacecraft developed slight aerodynamic and mass asymmetries just prior to reaching the primary data region. These asymmetries complicated the determination of the angle of attack by introducing biases in the angles of attack obtained by a force-accelerometer method normally used for that purpose. These biases are usually small and have generally been neglected in most previous work. However, because of the accuracy requirement of this experiment, it was thus necessary to employ solutions of the linearized equations of motion to determine the magnitude of these biases.

SYMBOLS

A_X, A_Y, A_Z accelerations parallel to X, Y, and Z body axes, respectively, g units

C_m pitching-moment coefficient

C_{m_o} incremental pitching-moment coefficient due to asymmetry

C_Y side-force coefficient

C_{Y_o}, C_{Z_o} incremental force coefficients due to asymmetries along Y and Z body axes, respectively

$C_{Y_{p_\alpha}} = \dfrac{\partial C_Y}{\partial\left(\dfrac{pd}{2V}\right)\partial\alpha}$ Magnus force coefficient along Y body axis, per radian^2

$C_{Y_r} = \dfrac{\partial C_Y}{\partial\left(\dfrac{rd}{2V}\right)}$ damping-force coefficient along Y body axis, per radian

$C_{Y_\beta} = \dfrac{\partial C_Y}{\partial\beta}$ side-force-coefficient slope, -1.985 per radian

C_Z normal-force coefficient

$C_{Z_{p_\beta}} = \dfrac{\partial C_Z}{\partial\left(\dfrac{pd}{2V}\right)\partial\beta}$ Magnus force coefficient along Z body axis, per radian^2

$C_{Z_q} = \frac{\partial C_Z}{\partial\left(\frac{qd}{2V}\right)}$ damping-force coefficient along Z body axis, per radian

$C_{Z_\alpha} = \frac{\partial C_Z}{\partial \alpha}$ normal-force-coefficient slope, -1.985 per radian

d reference diameter, 2.275 feet (0.693 meter)

h altitude, feet (meters)

m mass, slugs (kilograms)

$m' = \frac{mV}{\bar{q}S}$, seconds

p,q,r angular velocities about X, Y, and Z body axes, respectively, degrees/second

$\bar{q}$ dynamic pressure, pounds/foot^2 (newtons/meter^2)

S reference area, 4.06 feet^2 (0.377 meter^2)

t elapsed flight time, seconds

V earth-relative velocity, feet/second (meters/second)

W sea-level weight, 600.191 pounds (2669.782 newtons)

X,Y,Z orthogonal body axis system with origin at center of gravity

x,y,z distances along X-, Y-, and Z-axis, respectively, feet (meters)

x_o longitudinal position referenced to center of gravity of incremental force due to asymmetry, feet (meters)

α angle of attack, degrees

α^* in-plane angle of attack, degrees

α_o angle of attack at which normal-force coefficient is zero, degrees

β angle of sideslip, degrees

β_o angle of sideslip at which side-force coefficient is zero, degrees

β^* in-plane angle of sideslip ($\beta^* \approx \beta$), degrees

η total angle of attack, degrees

ρ density, slugs/foot^3 (kilograms/meter^3)

ρ_0 sea-level density, slugs/foot^3 (kilograms/meter^3)

Subscripts:

cg center of gravity

st static trim

t dynamic trim

T thermal

A dot over a symbol indicates derivative with respect to time.

TEST AND MEASUREMENTS

The Reentry F vehicle consisted of a three-stage Scout launch vehicle and the reentry spacecraft. (See ref. 1.) The spacecraft was a 13-foot-long (3.96-meter), 5^o half-angle cone with a graphite nose tip having a radius of 0.10 inch (2.54 mm). The skin served as the load-bearing structure and was made of seven individual conical frustums. Each frustum was made of beryllium and had a skin thickness of 0.6 inch (15.24 mm).

The Scout launched the Reentry F spacecraft into a precise ballistic trajectory along the NASA Wallops Station test range. Prior to separation the spacecraft was spun up to approximately 1 Hz to minimize the effects of any separation anomalies. The spacecraft was separated from the third stage of the Scout by a spring mechanism at t = 423.10 seconds, h = 314 942 feet (95 994.3 meters) and V = 19 572 ft/sec (5965.5 m/sec) and reentered the earth's atmosphere downrange near Bermuda.

Physical Characteristics and Ground Tests

A sketch of the Reentry F spacecraft and its associated axis systems is shown in figure 1. The mass and inertial characteristics were measured after the spacecraft had been mass balanced (ref. 2) at Wallops Station, Virginia, to approximately 500 oz-in^2 (91 kg-cm^2) (principal-axis tilt angle was approximately 2.877×10^{-5} radian).

No wind-tunnel tests were performed to determine the basic aerodynamics of the spacecraft because of its classical shape. The aerodynamics of reference 3 were used in the analysis of this report.

Flight Tests

Immediately after separation the spacecraft experienced a maximum total angle of attack of approximately 2° because of residual angular momentum and/or tipoff impulse. This value was determined by methods outlined in reference 4. This method involved simultaneous numerical integration of the Euler equations by using measured rate data to yield time histories of the spacecraft attitude angles which were then correlated with the flight-path angles of the spacecraft determined from radar tracking data. The initial conditions for this determination were obtained from the Scout guidance system. The total angle-of-attack envelope then damped as the spacecraft entered the denser atmosphere.

The continuous-motion instrumentation in the spacecraft consisted of three rate gyros and five linear accelerometers. The commutated-motion instrumentation consisted of three rate gyros and two linear accelerometers. The ranges and the locations of the accelerometers and rate gyros are listed in table 1. A reproduction of part of the Reentry F telemetry record showing the continuous channel motion data from spinup to signal loss is presented in figure 2. It may be discerned from the figure that as the trim angle-of-attack buildup due to asymmetries occurs, the accelerometer and rate-gyro data in the transverse plane (A_Y, A_Z, q, and r) exceed their respective instrument calibration limits. The coarse sensors with commutated output furnished the data during these periods. These composite data were then smoothed by use of a numerical filtering technique (ref. 5). In addition, the smoothed rate-gyro data were numerically differentiated and used to correct the measured accelerations to center-of-gravity values by using the accelerometer equations in reference 6. These smoothed and corrected data are presented in figures 3 and 4. Meteorological measurements of atmospheric properties were obtained with sonde payloads carried to altitude by special high-altitude sonde balloons and Arcas rockets (ref. 1). Free-stream density was derived from these data and is presented in figure 5. The derived density was combined with velocity from the spacecraft trajectory (ref. 1) to calculate the dynamic pressure presented in figure 6 with the trajectory data.

It can be seen in figures 2, 3, and 4 that the amplitude of the oscillations about trim of the transverse instrument data (q, r, A_Y, and A_Z) increases significantly after $t = 456.5$ seconds. In the presence of the positive dynamic-pressure gradient the spacecraft was experiencing, this divergence suggests a dynamic instability (ref. 7). This instability persists for approximately 2 seconds.

METHODS OF ANALYSIS

Force Method

The force method uses accelerometer data and a priori knowledge of the spacecraft aerodynamics to determine the angle of attack. An accelerometer at the center of gravity within a free-flight vehicle senses only the sum of the external forces acting on it. For a spacecraft without thrust, the only external forces are aerodynamic. The general expressions for the two accelerometers of interest A_Y and A_Z are

$$WA_{Z,cg} = \left[C_{Z_o} + C_{Z_\alpha}\alpha + C_{Z_q}\left(\frac{qd}{2V}\right) + C_{Z_{p_\beta}}\beta\left(\frac{pd}{2V}\right)\right]\bar{q}S \tag{1}$$

$$WA_{Y,cg} = \left[C_{Y_o} + C_{Y_\beta}\beta + C_{Y_r}\left(\frac{rd}{2V}\right) + C_{Y_{p_\alpha}}\alpha\left(\frac{pd}{2V}\right)\right]\bar{q}S \tag{2}$$

If the spacecraft is symmetrical and has a high reentry velocity and a low roll rate, the forces due to asymmetries, damping, and Magnus effects, respectively, may be neglected. Thus, α and β may be obtained from equations (1) and (2) as

$$\alpha = \frac{WA_{Z,cg}}{\bar{q}SC_{Z_\alpha}} \tag{3}$$

$$\beta = \frac{WA_{Y,cg}}{\bar{q}SC_{Y_\beta}} \tag{4}$$

These equations suffice for the determination of the angle of attack for most reentry spacecraft. But the Reentry F spacecraft did experience a trim buildup, and hence, the effect of asymmetries must be examined. A slight asymmetry on the nose of the cone in figure 7(a) might be caused by an uneven loss of material and/or body bending due to unsymmetrical heating. The effect of such an asymmetry is to superimpose a small incremental force coefficient on the basic normal-force-coefficient curve as shown in figure 7(b). Although the incremental force coefficient may be nonlinear over a relatively large range of α, it is a constant for a small range of α, as illustrated in figure 7(c), an enlargement of the inset of figure 7(b). This constant incremental force

coefficient is commonly referred to symbolically as C_{Z_o} and effectively causes a translational shift of the normal-force-coefficient curve along the α-scale through a displacement designated α_o. For asymmetries in the horizontal plane, C_{Y_o} and β_o are obtained by a similar process. The terms α_o and β_o are not to be confused with the trim angle of attack and sideslip; they are new angles at which the normal- and side-force coefficients are equal to zero. The static trim angle of attack α_{st} as shown in figure 7(d) is the result of C_{Z_o} acting through a moment arm of x_o to produce a moment asymmetry C_{m_o}.

By returning now to the general expressions for the accelerometers and still neglecting the forces due to damping and Magnus effects but considering asymmetries, equations (1) and (2) become

$$WA_{Z,cg} = \left(C_{Z_o} + C_{Z_\alpha}\alpha\right)\bar{q}S \tag{5}$$

$$WA_{Y,cg} = \left(C_{Y_o} + C_{Y_\beta}\beta\right)\bar{q}S \tag{6}$$

From figure 7(c), it is clear that

$$C_{Z_o} = -C_{Z_\alpha}\alpha_o \tag{7}$$

$$C_{Y_o} = -C_{Y_\beta}\beta_o \tag{8}$$

Substituting equations (7) and (8) into equations (5) and (6), respectively, yields

$$\alpha - \alpha_o = \frac{WA_{Z,cg}}{\bar{q}SC_{Z_\alpha}} \tag{9}$$

$$\beta - \beta_o = \frac{WA_{Y,cg}}{\bar{q}SC_{Y_\beta}} \tag{10}$$

Thus, when asymmetries are considered, the force method yields an "angle of attack" and an "angle of sideslip" which are, in effect, biased by the previously mentioned shift in the normal-force-coefficient curve. The magnitude of this shift cannot be ascertained from the accelerometer data alone. However, a method is presented in the next section which uses both accelerometer and rate-gyro data in the rate solution of the linearized equations of motion to determine the shift.

Method by Solution of Linearized Equations of Motion (SLEM)

The determination of the angle of attack by the force method has been presented in the preceding section. As pointed out therein, the angle of attack is biased by a translational shift in the normal-force-coefficient curve when asymmetries are considered.

This bias angle is usually small and normally has been neglected in most previous work. However, since the angle of attack of Reentry F is small (1^{o}), this bias angle cannot be ignored. The purpose of this section, then, is to describe the procedure used to determine the bias angle.

The angular-rate solution of the linearized equations of motion is presented in erence 8. Only the expressions dealing with body yaw-rate and pitch-rate trims are r quired for this method, and they are

$$r_t = p\alpha_t + \frac{C_{Z_\alpha}}{m'}\beta_t + \frac{C_{Y_o}}{m'} \tag{11}$$

$$q_t = p\beta_t - \frac{C_{Z_\alpha}}{m'}\alpha_t - \frac{C_{Z_o}}{m'} \tag{12}$$

With equations (7) and (8) and knowledge that $C_{Y_\beta} = C_{Z_\alpha}$ with the assumption of near symmetry, equations (11) and (12) may now be written as

$$r_t = p\alpha_t + \frac{C_{Z_\alpha}}{m'}(\beta_t - \beta_o) \tag{13}$$

$$q_t = p\beta_t - \frac{C_{Z_\alpha}}{m'}(\alpha_t - \alpha_o) \tag{14}$$

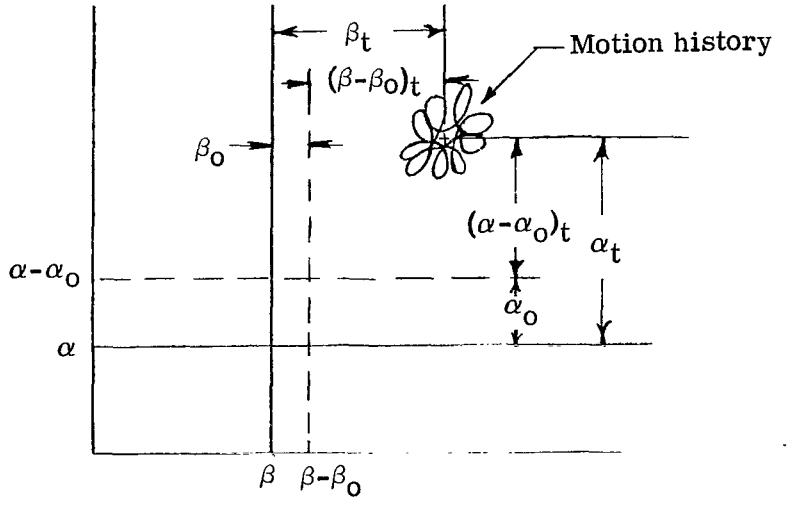

Sketch (a)

In sketch (a) it can be seen that

$$(\alpha - \alpha_o)_t = \alpha_t - \alpha_o \tag{15}$$

$$(\beta - \beta_o)_t = \beta_t - \beta_o \tag{16}$$

Thus, equations (13) and (14) become

$$r_t = p\alpha_t + \frac{C_{Z_\alpha}}{m'}(\beta - \beta_o)_t \tag{17}$$

$$q_t = p\beta_t - \frac{C_{Z_\alpha}}{m'}(\alpha - \alpha_o)_t \tag{18}$$

Examination of equations (17) and (18) reveals that for given values of q_t, r_t, and p (estimated from the flight data) and reduced values of $(\alpha - \alpha_o)_t$ and $(\beta - \beta_o)_t$ (from the force method), values of α_t and β_t may be calculated. From equations (15) and (16), α_o and β_o may be determined. And finally, α and β may be computed by adding α_o and β_o to the respective time histories of $\alpha - \alpha_o$ and $\beta - \beta_o$ determined by the force method.

RESULTS AND DISCUSSION

Force Method

The results of computing the motion time history by the force method are shown in figure 8. These results were used in the preliminary analysis of reference 1. For the purposes of that paper, however, $\alpha - \alpha_o$ and $\beta - \beta_o$ were rotated from the motion instrument axis system to the thermal axis system (fig. 1).

Force-SLEM Method

Values of q_t, r_t, $(\alpha - \alpha_o)_t$, and $(\beta - \beta_o)_t$ were estimated from time histories and crossplots of the data and the results of the force method. The mean values of the time histories were assumed to be the trim values. On each crossplot the center of any discernible pattern was designated as the trim. A third procedure made use of the fact that under the assumed conditions of SLEM $\left(A_X = \dot{p} = \dot{\bar{q}} = 0\right)$, the instantaneous trim center would be marked in the crossplots by the intersection of the bisectors of any three successive loops of a motion pattern. Sketch (b) presents a typical example of this method. The advantage of this method was that the entire motion pattern was not necessary to estimate a trim center. Although the assumed conditions of SLEM are not met in flight, they are approximated for short time periods (1 second). The estimated trim values from the three procedures are presented in figure 9. These values were faired and used in equations (17) and (18) to solve for α_t and β_t. These were used in turn in equations (15) and (16) to determine α_o and β_o. These results are shown in figure 10. An indication that the Reentry F spacecraft had multiple asymmetries and/or a bent body

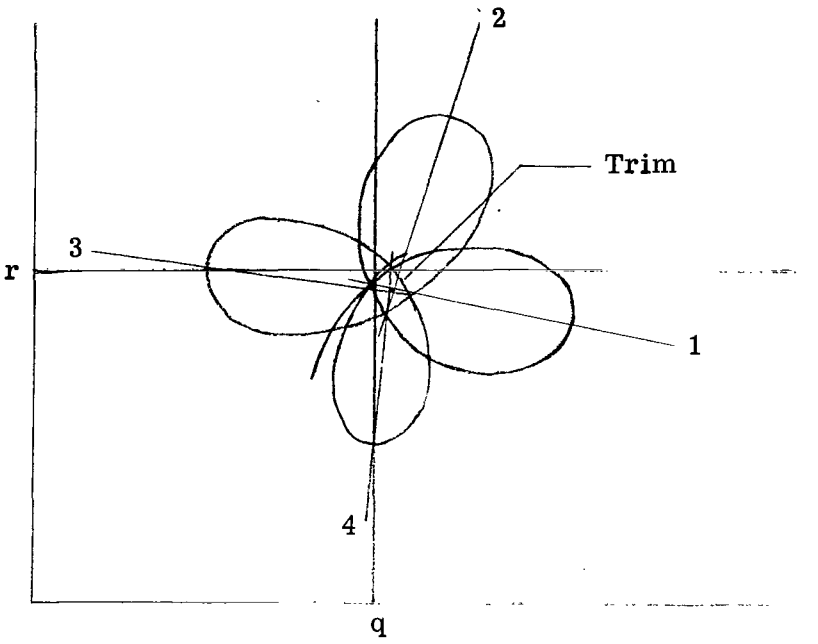

Sketch (b)

can be noted in this figure. The situation which occurs, for example, at $t = 456$ seconds where $\alpha_o \cong 0$ while $\alpha_t = 0.15^o$ could not exist for the case of a single asymmetry, and would imply that it is possible to have a trimming moment with no force due to an asymmetry. In sketch (c) if $\left|\left(C_{Z_o}\right)_1\right| = \left|\left(C_{Z_o}\right)_2\right|$, the forces due to asymmetries will cancel $\left(\Sigma C_{Z_o} = 0\right)$, whereas the trimming moments will add. For Reentry F at $t = 456$ seconds (fig. 10), it appears there too that $\Sigma C_{Z_o} = 0$; the $\Sigma C_{Z_o} x_o$ are either adding or unbalanced in such a manner that the resultant moment is not equal to zero.

The values of α_o and β_o were added to the results of the force method and are presented in figure 11. These results are also presented in figure 12 as a crossplot time history of α against β. The purpose of this figure is to show the simultaneous dynamics of both the trim and oscillatory parts which make up the total angle of attack. The pitch-roll resonance region characterized by nonprecessing, overlapping circular motions at $t = 447$ to 450 seconds is well illustrated in the figure. The lack of apparent amplification of the motions during resonance indicates that the spacecraft had no asymmetries prior to that time. However, as the spacecraft emerges from resonance, a slight negative trim angle of attack (-0.07^o) may be discerned. Between $t = 454$ and 455 seconds, the trim experiences a reversal in orientation and a subsequent rapid growth in the same general direction to a maximum α_t of 0.87^o at $t = 460$ seconds. An apparent dynamic instability of the oscillatory part of the angle of attack occurs from $t = 456.5$ to

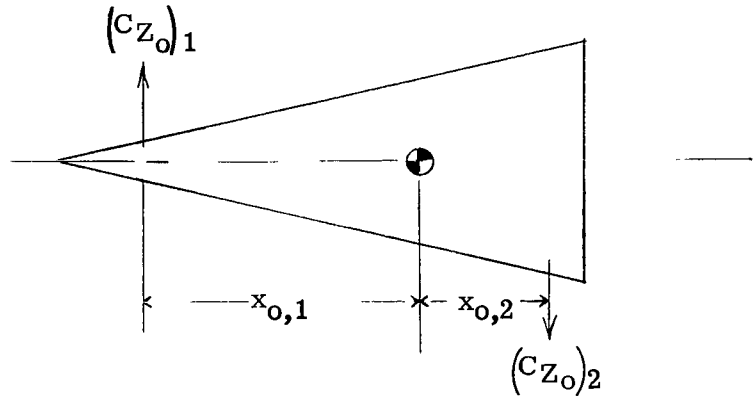

Sketch (c)

458.8 seconds. After that time the oscillatory part damps quite rapidly leaving the spacecraft with an angle of attack which is mostly due to trim.

These results have been computed with respect to the body axis system. Since the thermal-experiment instrumentation is located in the thermal axis system, α and β have been transformed to that axis system and are presented in figure 13. In addition, α_t and β_t were transformed to the thermal axis system and are presented in figure 14. The following single-rotation equations were used:

$$\alpha_T = \alpha \cos 7.5^o - \beta \sin 7.5^o$$

$$\beta_T = \beta \cos 7.5^o + \alpha \sin 7.5^o$$

As a point of interest, unpublished angles of attack computed by the pressure-differential method outlined in reference 9 with Reentry F pressure data are presented in figure 15. These angles are presented for stations 74.5, 100.5, and 145.5 inches (189.23, 255.27, and 369.57 cm) in the α-plane and station 145.5 in the β^*-plane. The envelopes of α and β computed by the combination force-SLEM method are over-plotted on the results of the pressure-differential method in figures 15(b) and 15(d), respectively. In general, there is good agreement between the results of the two methods until approximately $t = 456.5$ seconds. Since the low-range (0 to 3 psia) (0 to 20.7 kN/m^2 abs) pressure gages became saturated at that time, data from the high-range (0 to 20 psia) (0 to 137.9 kN/m^2 abs) gages were used thereafter to determine the angles of attack. Because the data from the high-range gages are inherently less accurate than the data from the low-range gages, it is believed that the agreement between the two methods deteriorates as a consequence.

Accuracy

Maximum errors in the rate-gyro and accelerometer measurements are estimated to be ±2 percent of the instrumentation full-scale range. Meteorological data are estimated to be accurate within approximately ±5 percent. Reference 3 presents experimental force and moment results of hypersonic wind-tunnel tests conducted in air, nitrogen, and helium on a family of slender cones with various nose bluntness ratios. The normal-force-coefficient slope C_{Z_α} for a slender cone with a zero nose bluntness ratio is estimated in reference 3 to be accurate within ±3.33 percent. The Reentry F spacecraft was a slender cone with a small nominal nose bluntness ratio (ratio of nose radius to base radius was 0.088) and flew at hypersonic velocities during its entire flight. The accuracy of the normal-force-coefficient slope of Reentry F, therefore, is also estimated to be within ±3.33 percent. Thus, the maximum error in the angles of attack, based on the assumptions of the combination force-SLEM method and the aforementioned accuracy of the instruments and the normal-force-coefficient slope, is estimated to be less than $\pm 0.1^{\circ}$.

CONCLUDING REMARKS

An analysis of the flight motions of the Reentry F spacecraft was made by the combination of the force method and an application of the angular-rate solution of the linearized equations of motion. The results of the analysis indicate the following:

1. No apparent amplification of the angle of attack occurred during pitch-roll resonance (447 to 450 seconds). This result indicates that little or no asymmetries were present prior to that time.

2. A slight negative trim angle of attack (-0.07°) is noted just after the spacecraft emerges from resonance at 451 seconds. Between 454 and 455 seconds, there is a reversal in orientation of the trim angle of attack and subsequently a rapid growth in the same general direction to a maximum of 0.87° at 460 seconds.

3. The payload experiences a dynamic instability from 456.5 to 458.7 seconds.

4. The Reentry F spacecraft had either multiple asymmetries or a bent body.

Langley Research Center,
National Aeronautics and Space Administration,
Hampton, Va., July 13, 1970.

REFERENCES

1. Rumsey, Charles B.; Carter, Howard S.; Hastings, Earl C., Jr.; Raper, James L.; and Zoby, Ernest V.: Initial Results From Flight Measurements of Turbulent Heat Transfer and Boundary-Layer Transition at Local Mach Numbers Near 15 (Reentry F). NASA TM X-1856, 1969.

2. Long, Moses J.: Balancing Considerations for Rocket Vehicles and Components. AIAA Sounding Rocket Vehicle Technology Specialist Conference, Feb.-Mar. 1967, pp. 423-429.

3. Harris, Julius E.: Force-Coefficient And Moment-Coefficient Correlations And Air-Helium Simulation for Spherically Blunted Cones. NASA TN D-2184, 1964.

4. Mayhue, Robert J.: Determination of Trajectory and Angles of Attack of a Scout Heat-Transfer Spacecraft During Reentry Flight in the Atmosphere. NASA TN D-2776, 1965.

5. Graham, Ronald J.: Determination and Analysis of Numerical Smoothing Weights. NASA TR R-179, 1963.

6. Lovelace, Uriel M.; Hoffman, Sherwood; and Mayhue, Robert J.: Analysis of the Trajectory and Large-Amplitude Motions of a Scout Vehicle During Fourth-Stage Reentry Flight. NASA TN D-2309, 1964.

7. Nicolaides, John D.; Eikenberry, Robert S.; and Ingram, Charles W.: The Determination of Aerodynamic Stability Coefficients From Sounding Rocket Flight Data. AIAA Sounding Rocket Vehicle Technology Specialist Conference, Feb.-Mar. 1967, pp. 257-270.

8. Woodbury, Gerard E.: Angle-of-Attack Analysis For Project Fire 1 Payload Reentry Flight. NASA TN D-3366, 1966.

9. Swalley, Frank E.: Measurement of Flow Angularity at Supersonic and Hypersonic Speeds With the Use of a Conical Probe. NASA TN D-959, 1961.

TABLE 1.- MOTION INSTRUMENTATION

Measurement	Range	Sampling rate (samples per second)	Location (measured from center of gravity)					
			x		y		z	
			ft	m	ft	m	ft	m
Pitch rate, high range	-20 to 20 deg/sec	60	0.3939	0.1201	-0.0971	-0.0296	-0.2133	-0.0650
Pitch rate, low range	-5 to 5 deg/sec	Continuous	.3939	.1201	.1887	.0575	-.2133	-.0650
Yaw rate, high range	-20 to 20 deg/sec	60	.3939	.1201	-.1887	-.0575	-.2133	-.0650
Yaw rate, low range	-5 to 5 deg/sec	Continuous	.3939	.1201	.0971	.0296	-.2133	-.0650
Roll rate, high range	-2000 to 2000 deg/sec	60	.3739	.1140	-.1479	-.0451	-.1349	-.0411
Roll rate, low range	-500 to 500 deg/sec	Continuous	.3739	.1140	.1379	.0420	-.1349	-.0411
Normal acceleration, high range	-10g to 10g	60	.6350	.1935	-.0510	-.0155	-.0810	-.0247
Normal acceleration, low range	-2g to 2g	Continuous	.7690	.2344	-.0510	-.0155	-.0810	-.0242
Lateral acceleration, high range	-10g to 10g	60	.8920	.2719	-.0150	-.0046	.0110	.0034
Lateral acceleration, low range	-2g to 2g	Continuous	1.0000	.3048	-.0150	-.0046	.0110	.0034
Longitudinal acceleration, high range	-40g to 2g	Continuous	.6830	.2082	.2940	.0896	.0110	.0034
Longitudinal acceleration, medium range	-10g to 2g	Continuous	.9220	.2810	-.1350	-.0411	.0110	.0034
Longitudinal acceleration, low range	-3g to 2g	Continuous	.9220	.2810	.1350	.0411	.0110	.0034

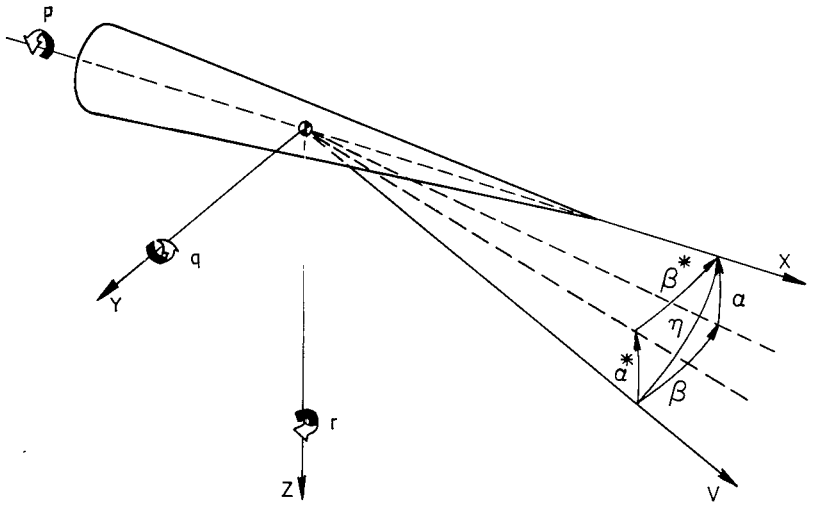

(a) Body axis system.

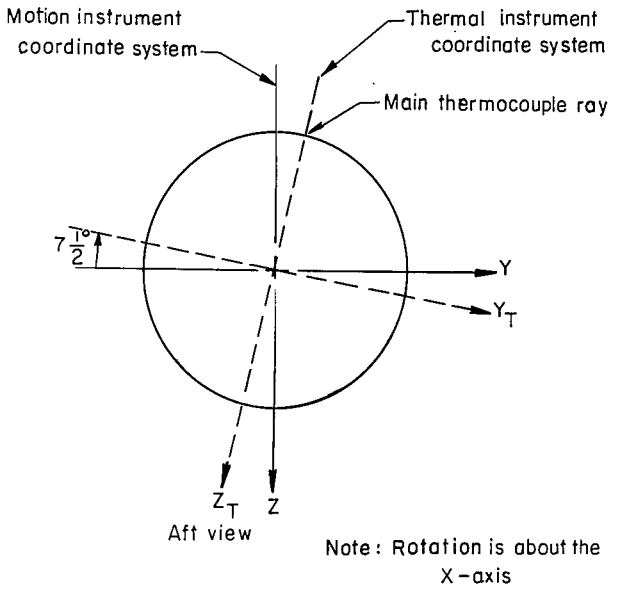

(b) Motion and thermal instrument axis systems.

Figure 1.- Axis systems.

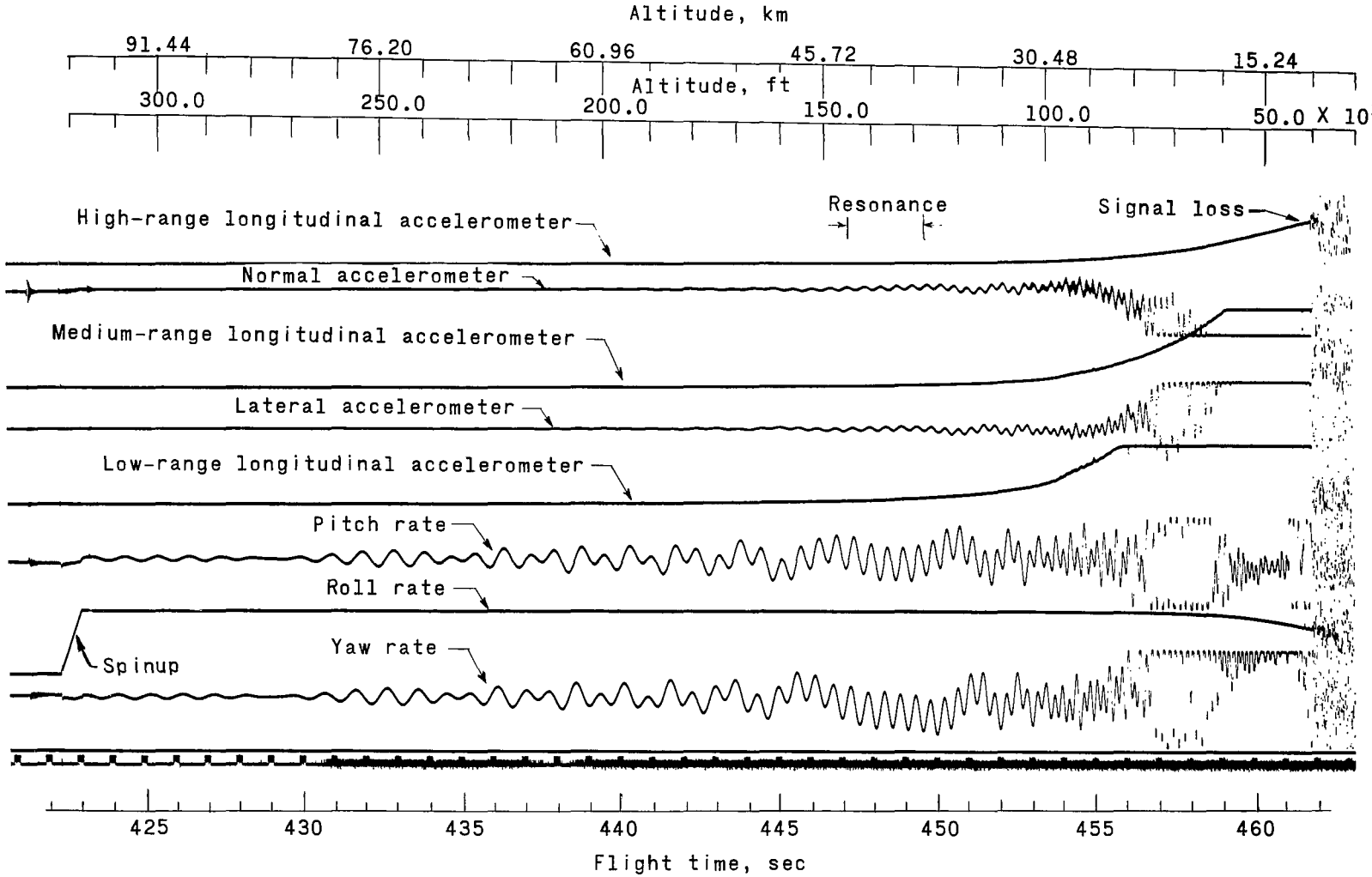

Figure 2.- Continuous channel motion data.

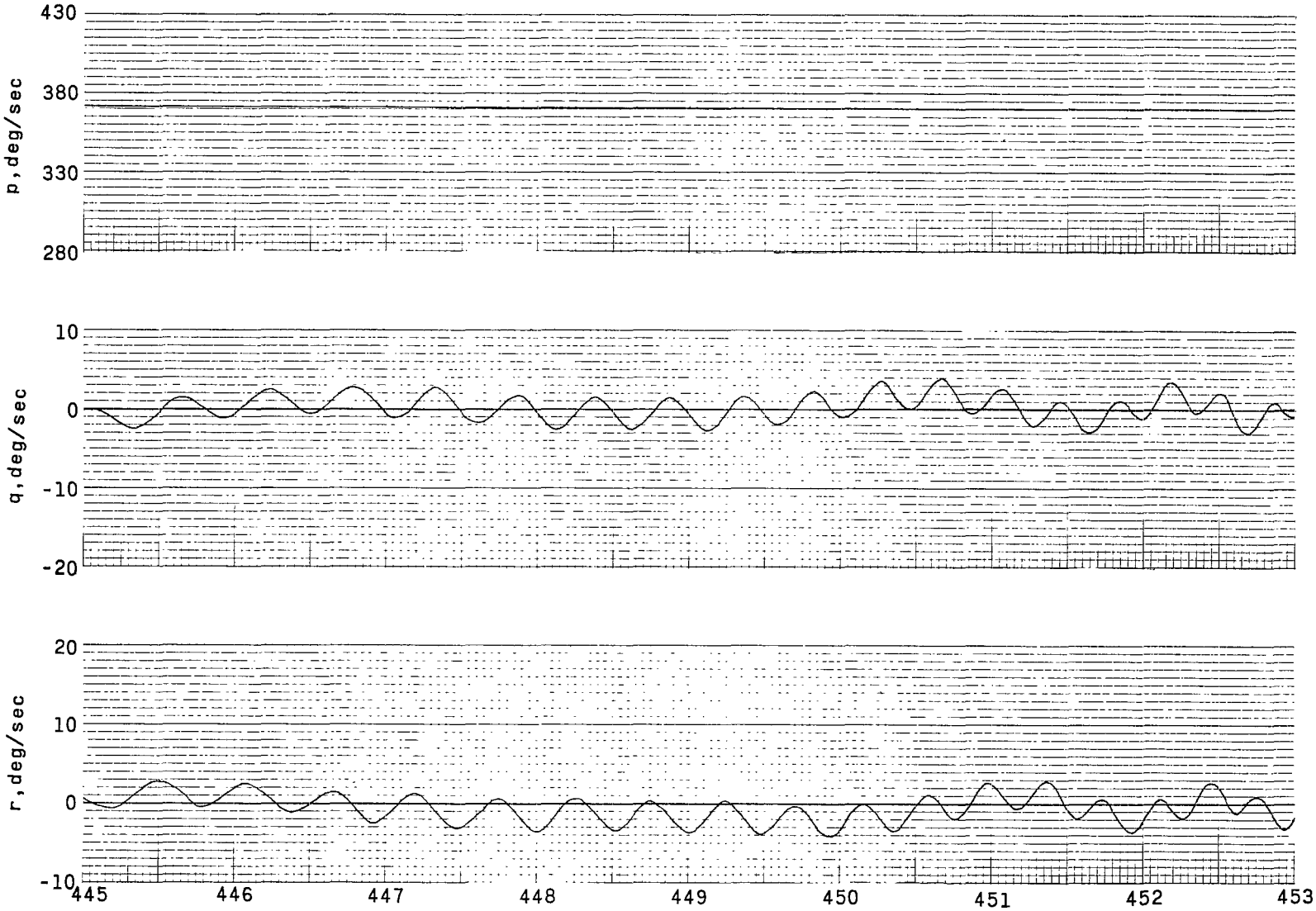

(a) Time = 445 to 453 seconds.

Figure 3.- Roll rate, pitch rate, and yaw rate as a function of time.

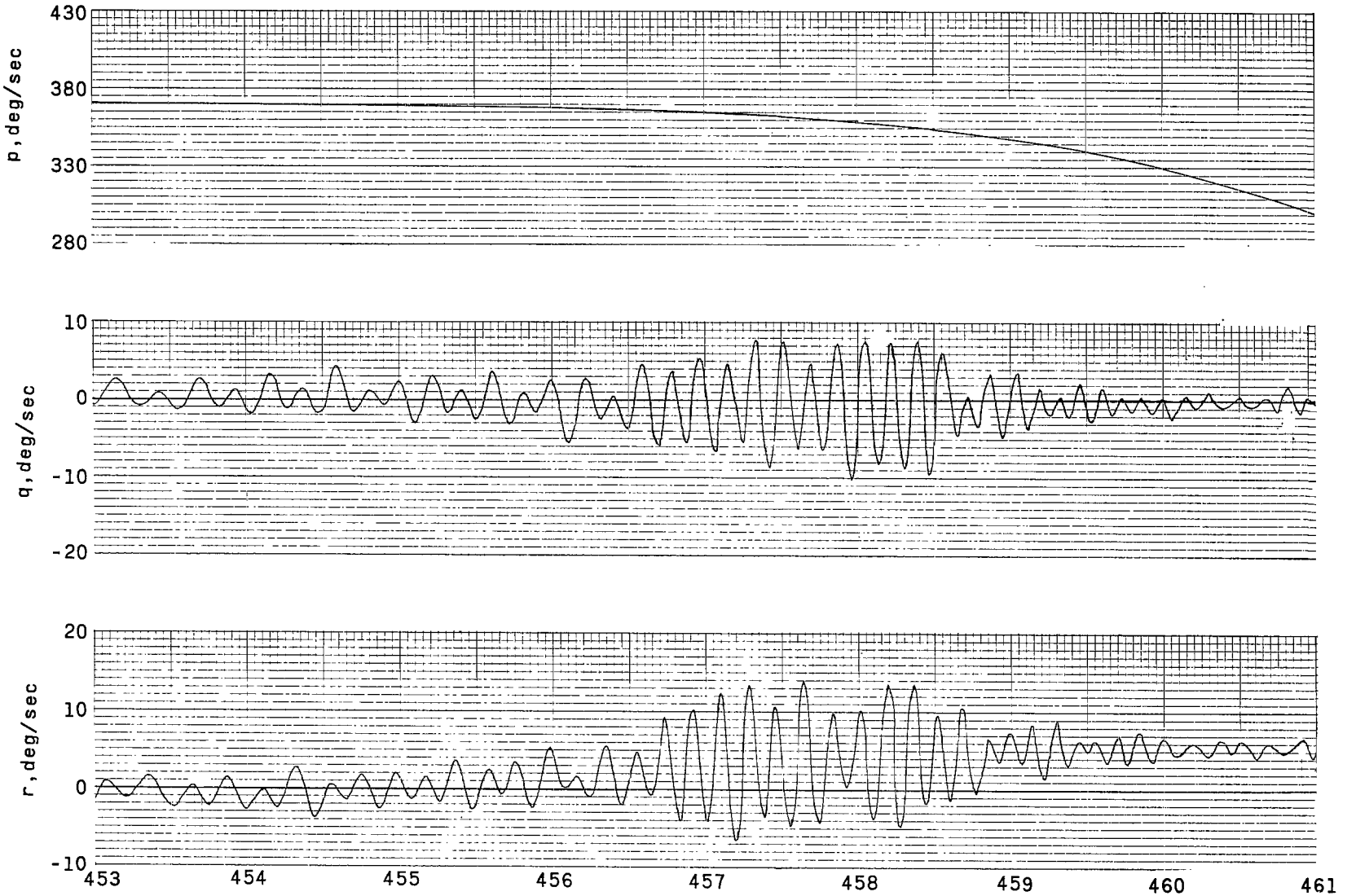

(b) Time = 453 to 461 seconds.

Figure 3.- Concluded.

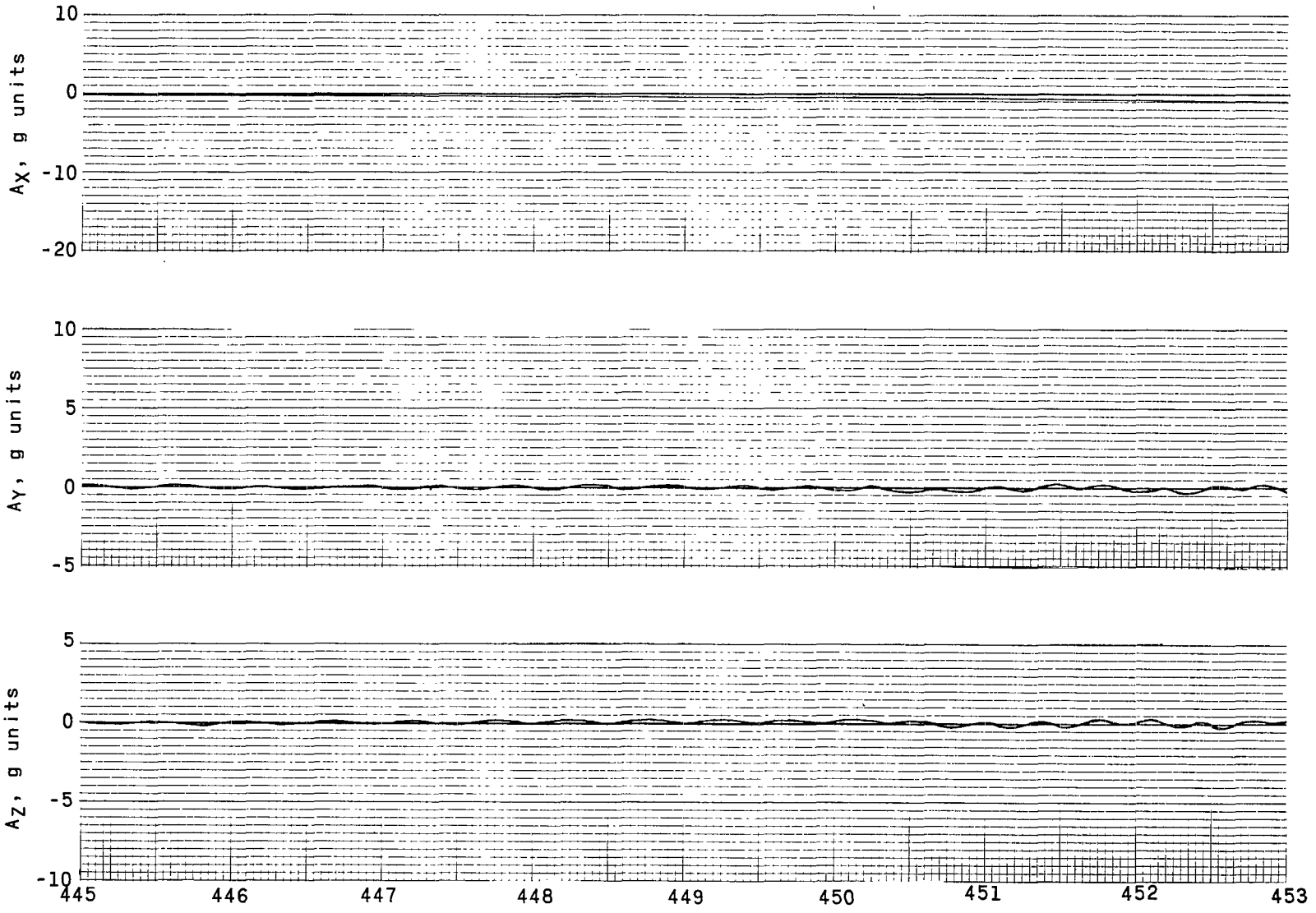

(a) Time = 445 to 453 seconds.

Figure 4.- Longitudinal, lateral, and normal accelerations as a function of time.

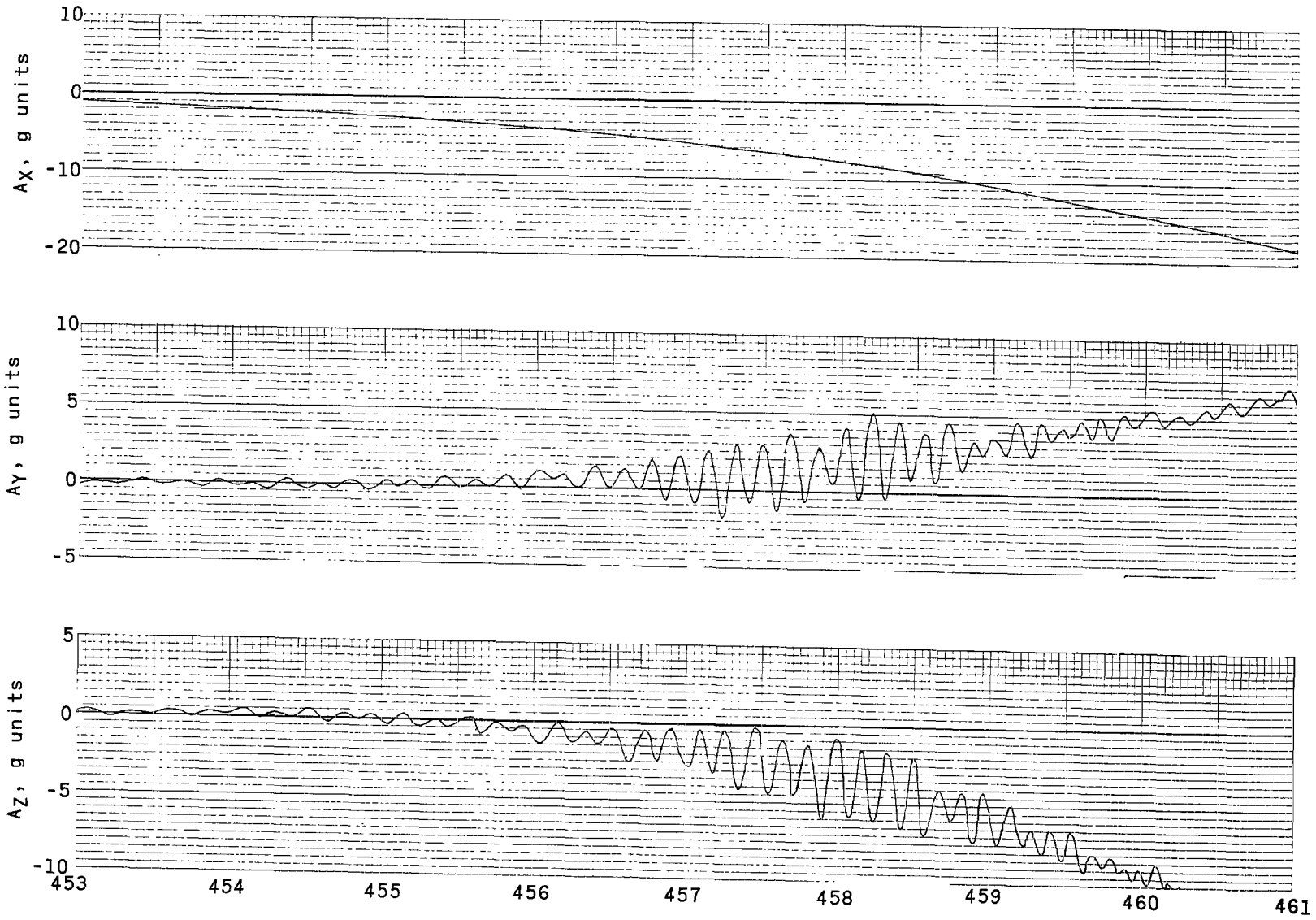

(b) Time = 453 to 461 seconds.

Figure 4.- Concluded.

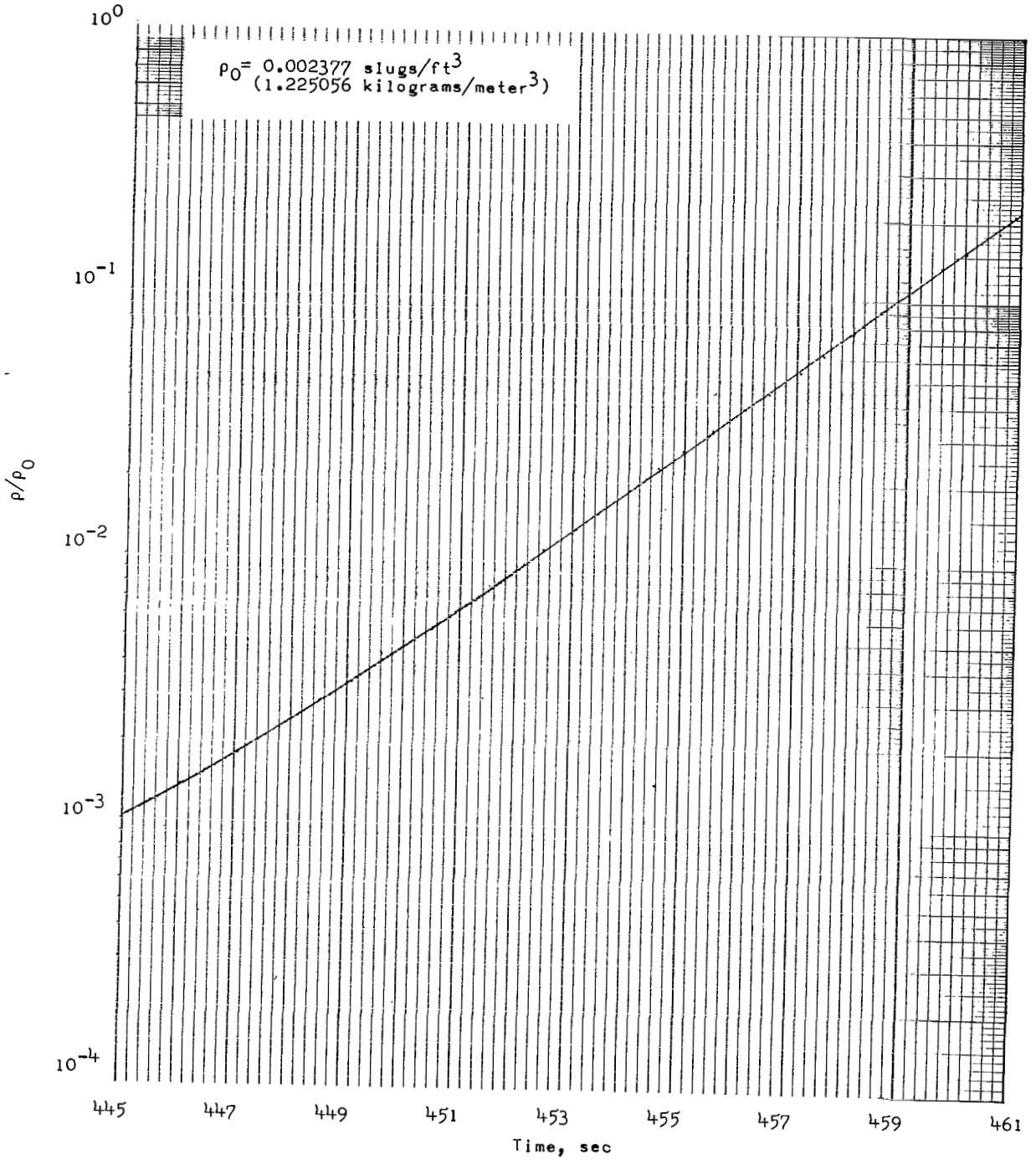

Figure 5.- Density time history.

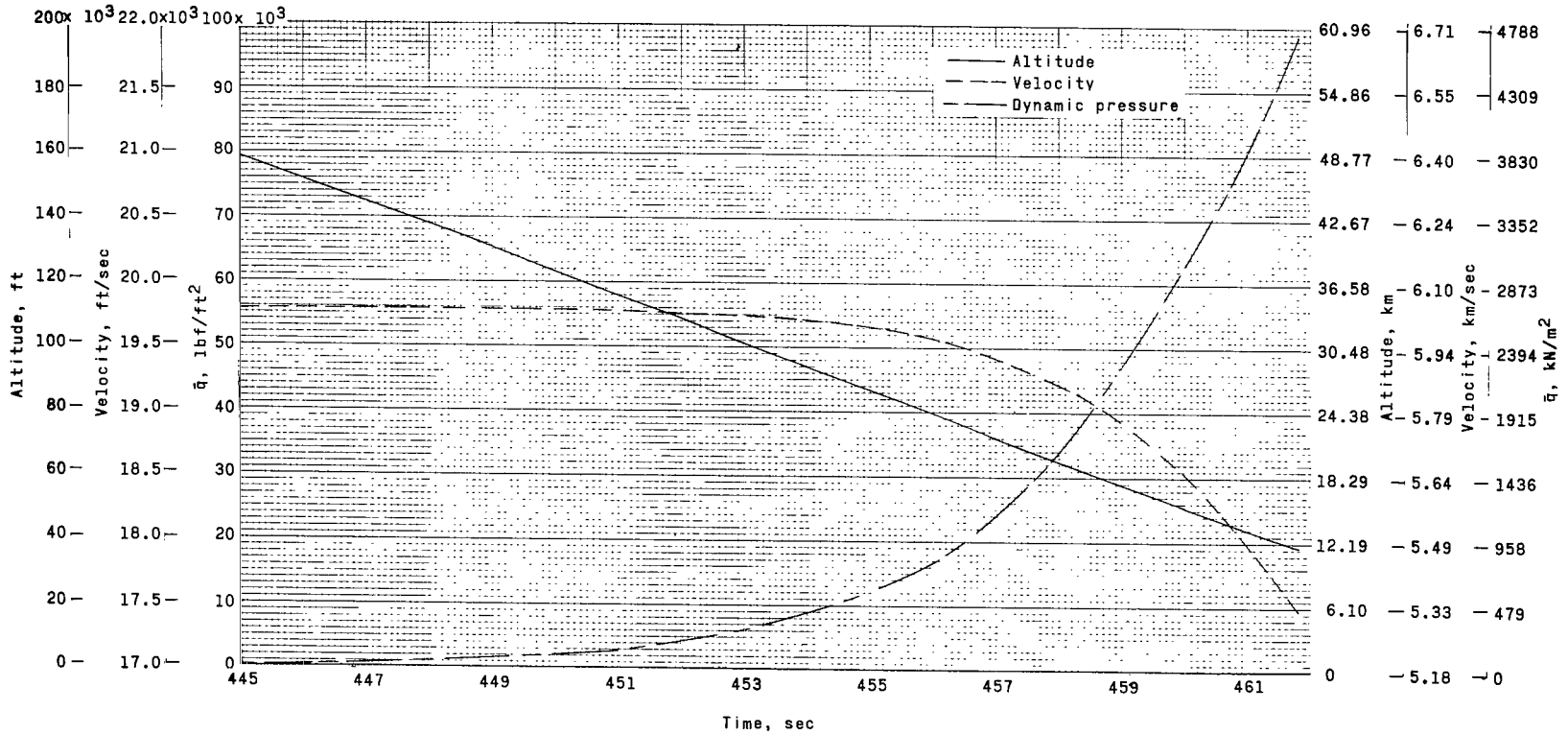

Figure 6.- Trajectory data as a function of time.

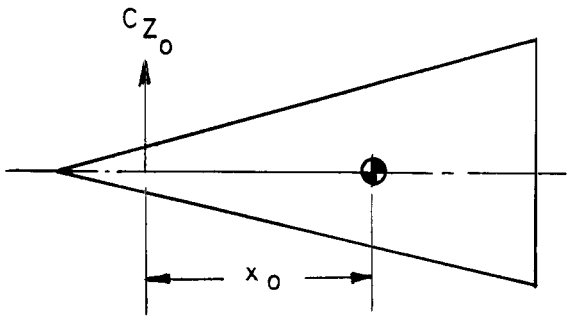

(a) Asymmetrical spacecraft.

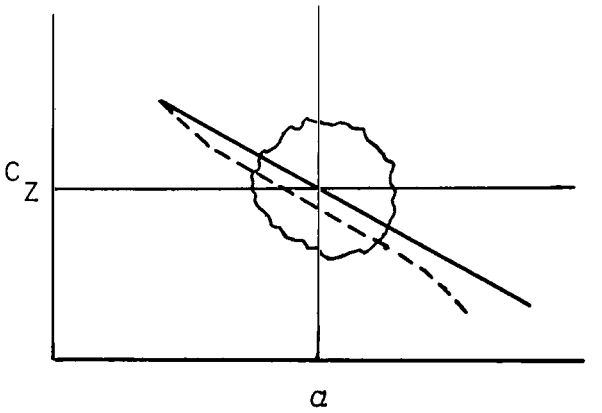

(b) Normal-force-coefficient curve.

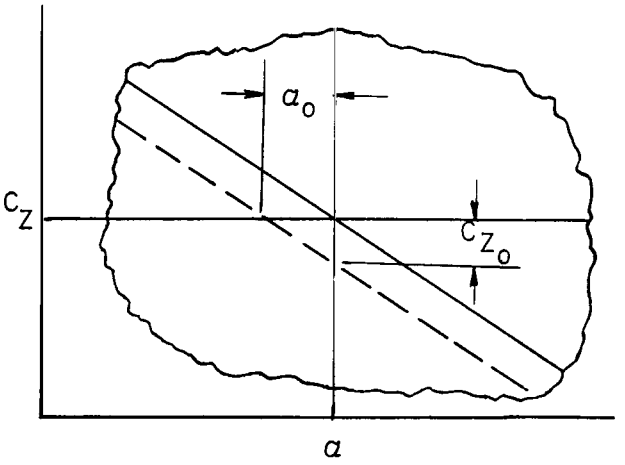

(c) Inset from normal-force-coefficient curve.

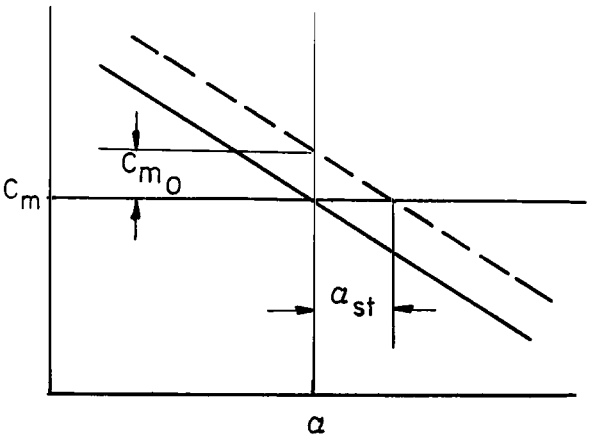

(d) Static trim angle of attack.

Figure 7.- Sketch illustrating the effects of slight asymmetry on spacecraft basic aerodynamics.

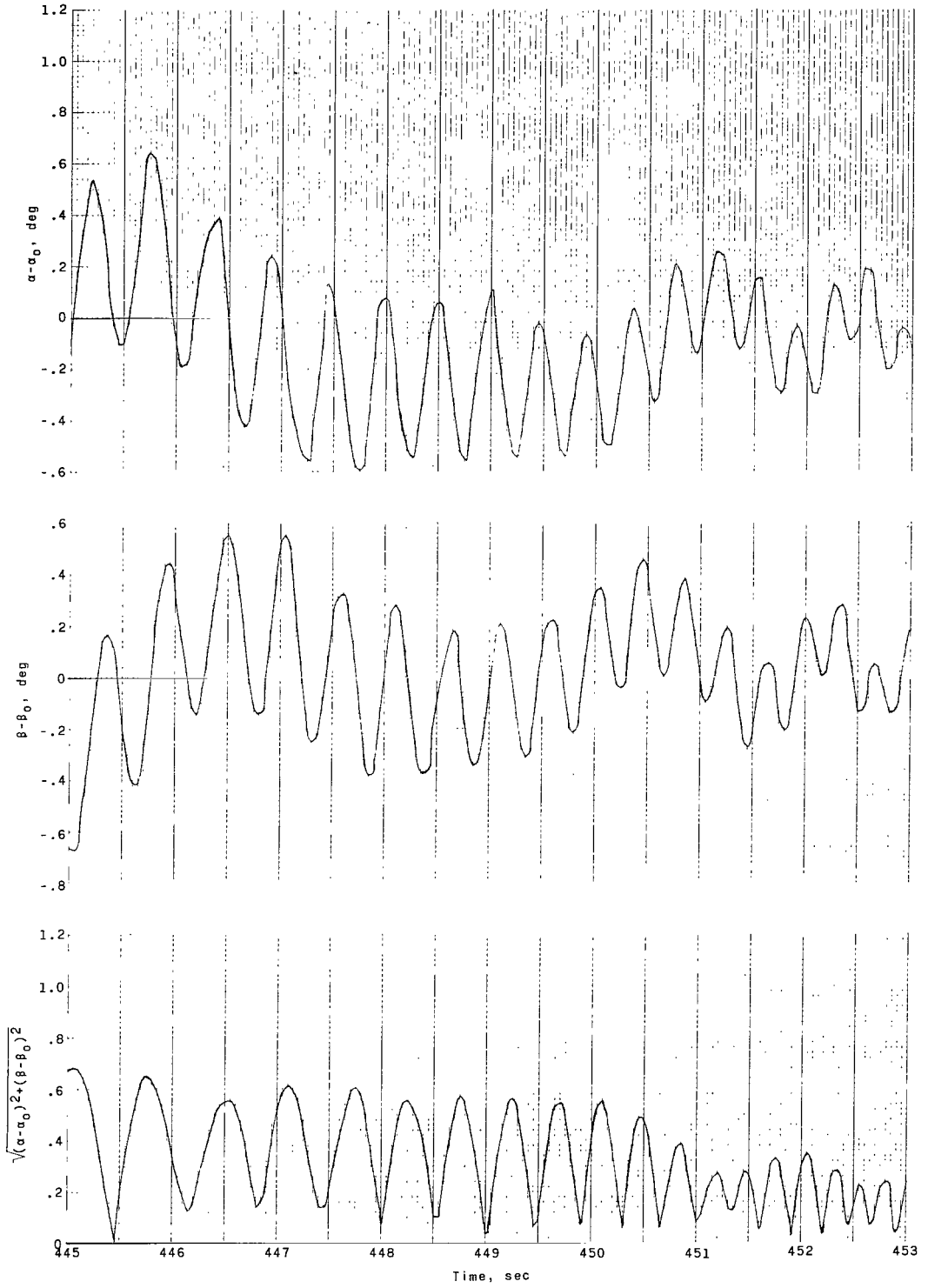

(a) Time = 445 to 453 seconds.

Figure 8.- Angle of attack, angle of sideslip, and total angle of attack as a function of time, determined by the force method.

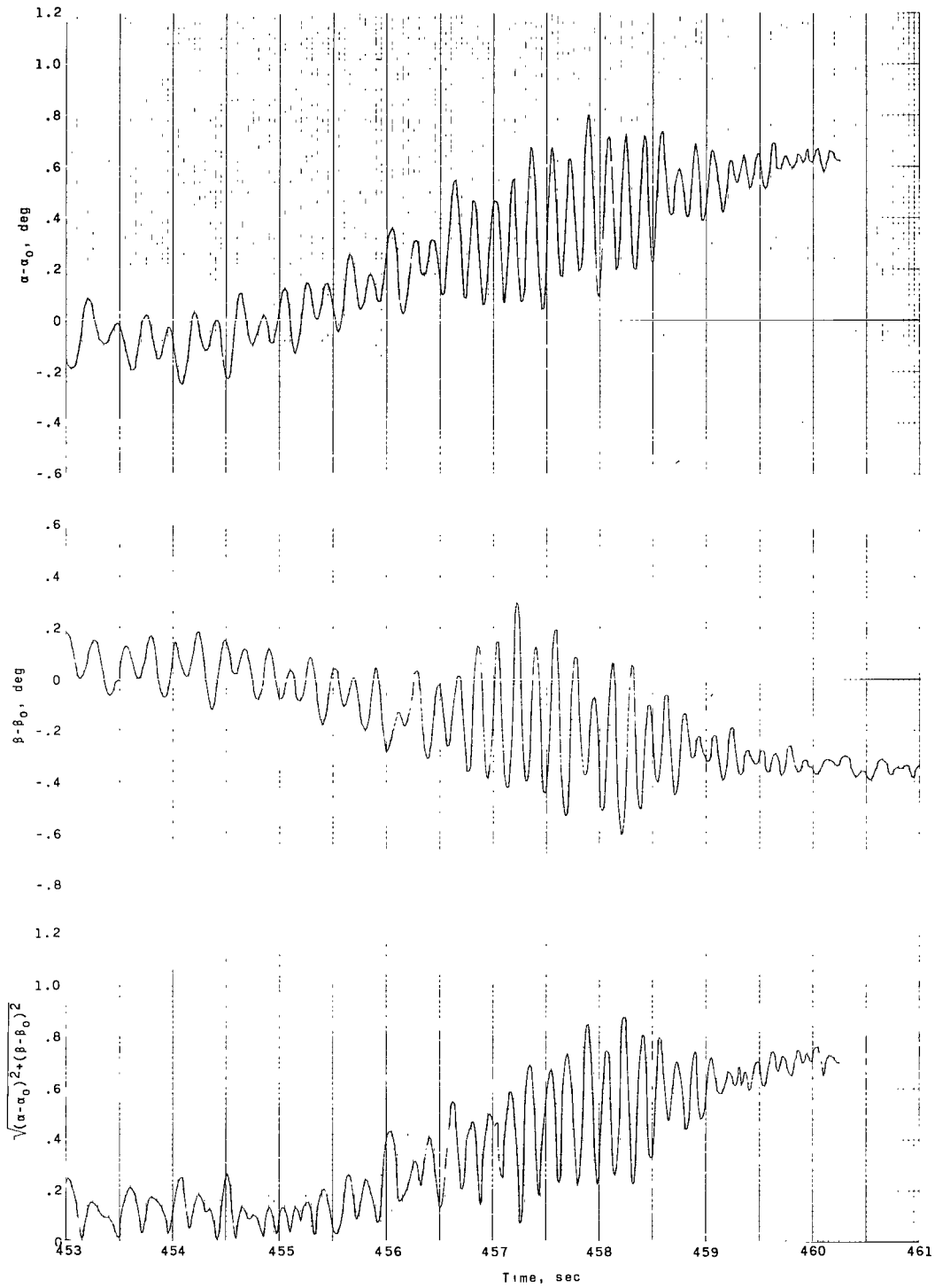

(b) Time = 453 to 461 seconds.

Figure 8.- Concluded.

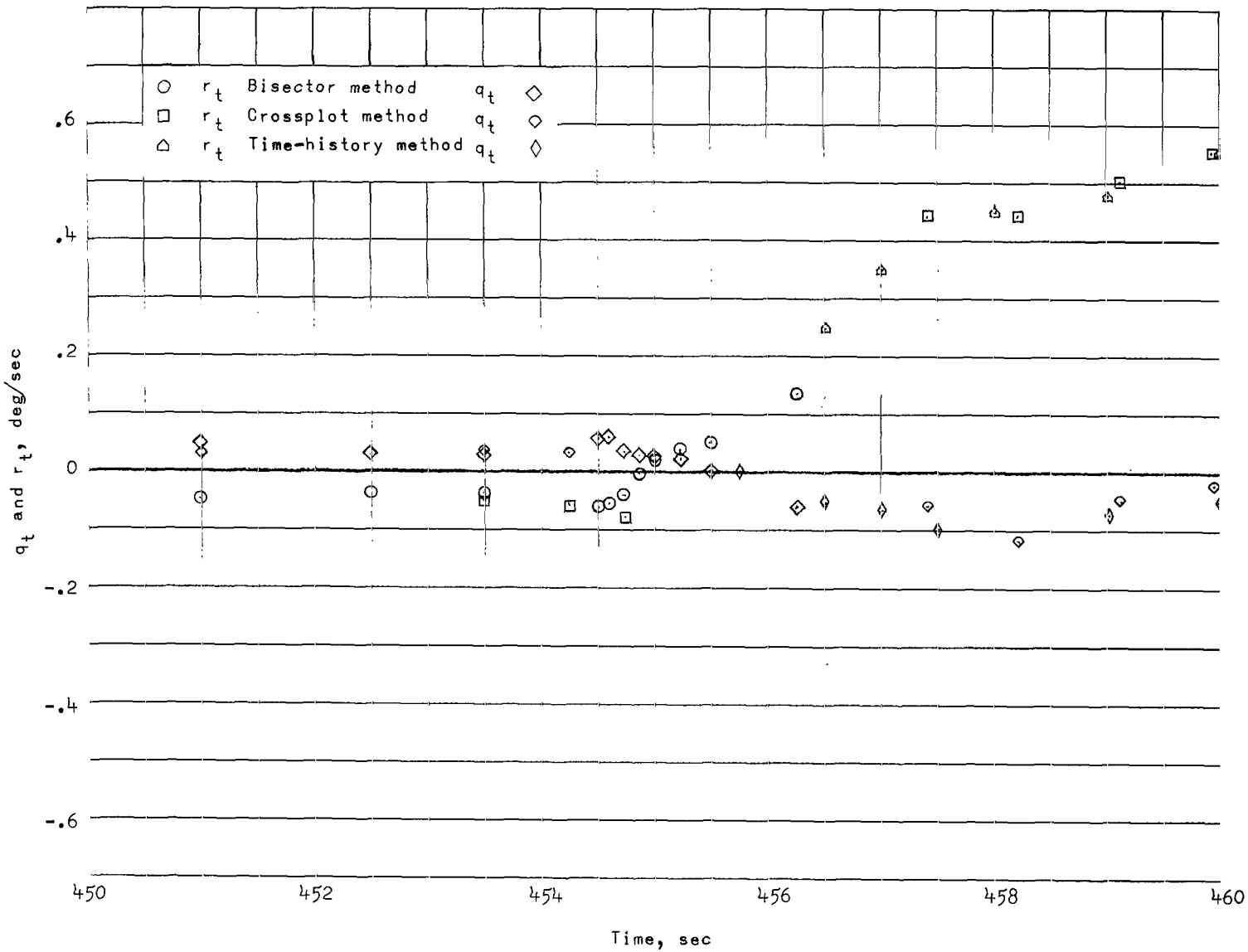

(a) q_t and r_t as a function of time.

Figure 9.- Estimated trim values.

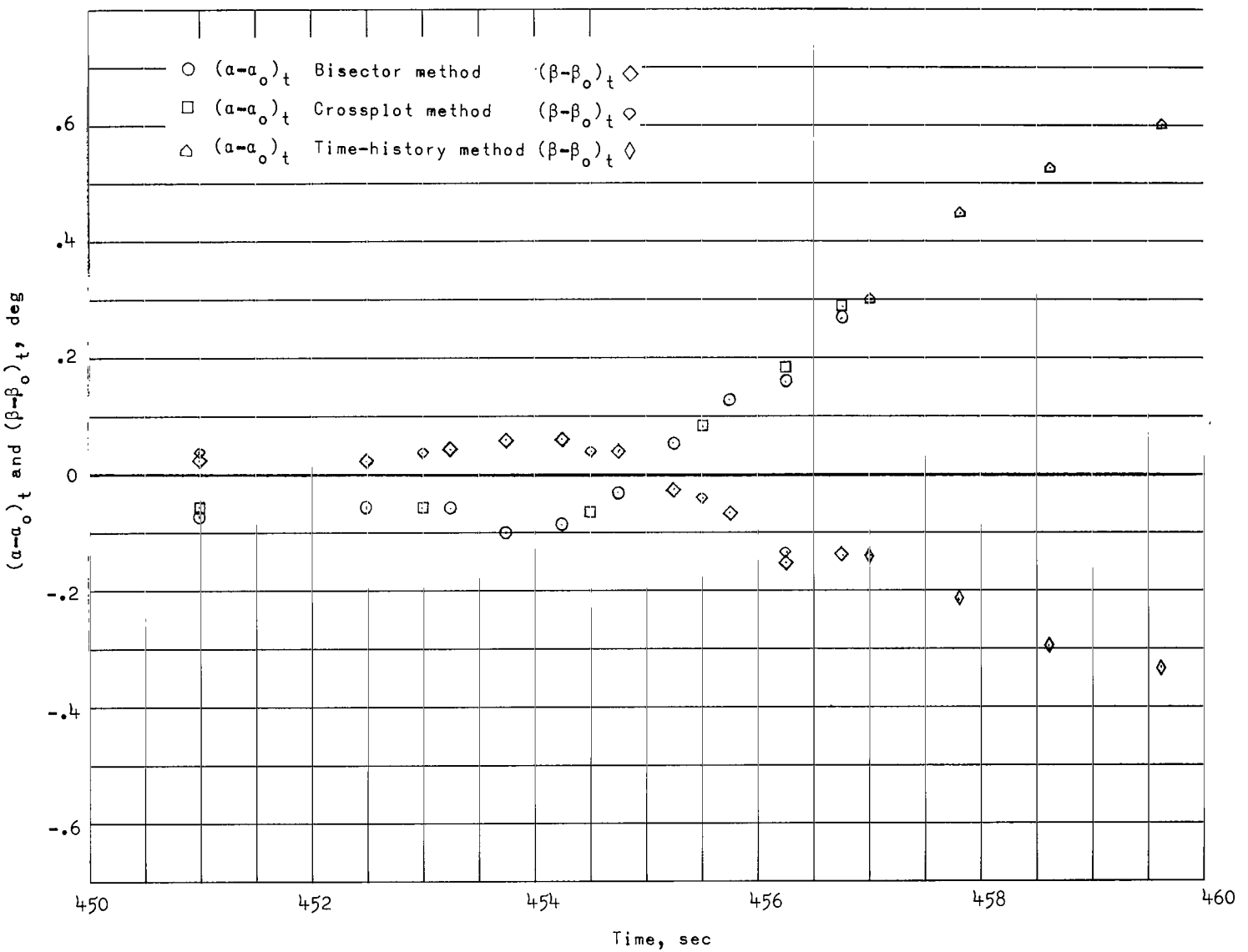

(b) $(\alpha - \alpha_o)_t$ and $(\beta - \beta_o)_t$ as a function of time.

Figure 9.- Concluded.

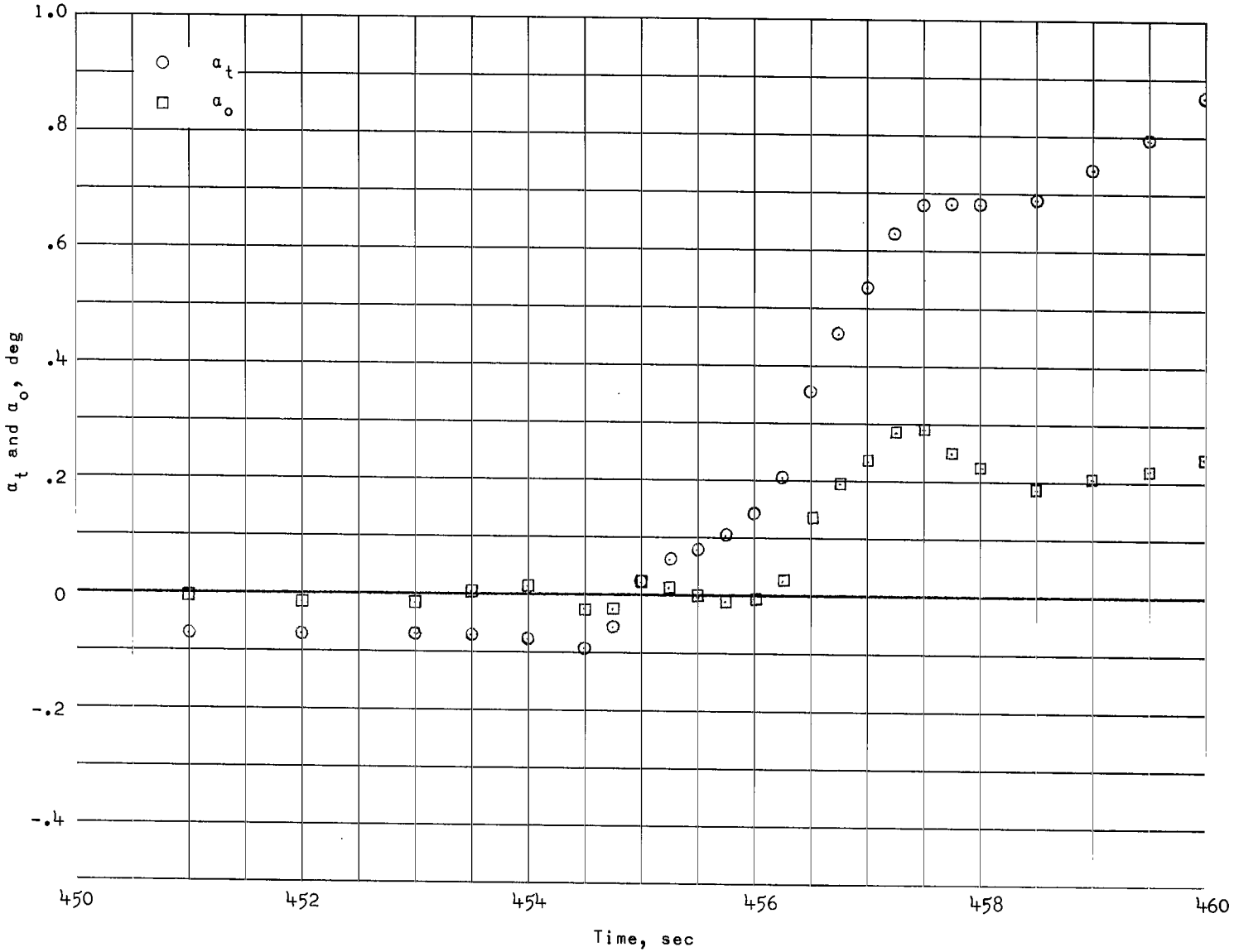

(a) α_t and α_o as a function of time.

Figure 10.- Computed trim values.

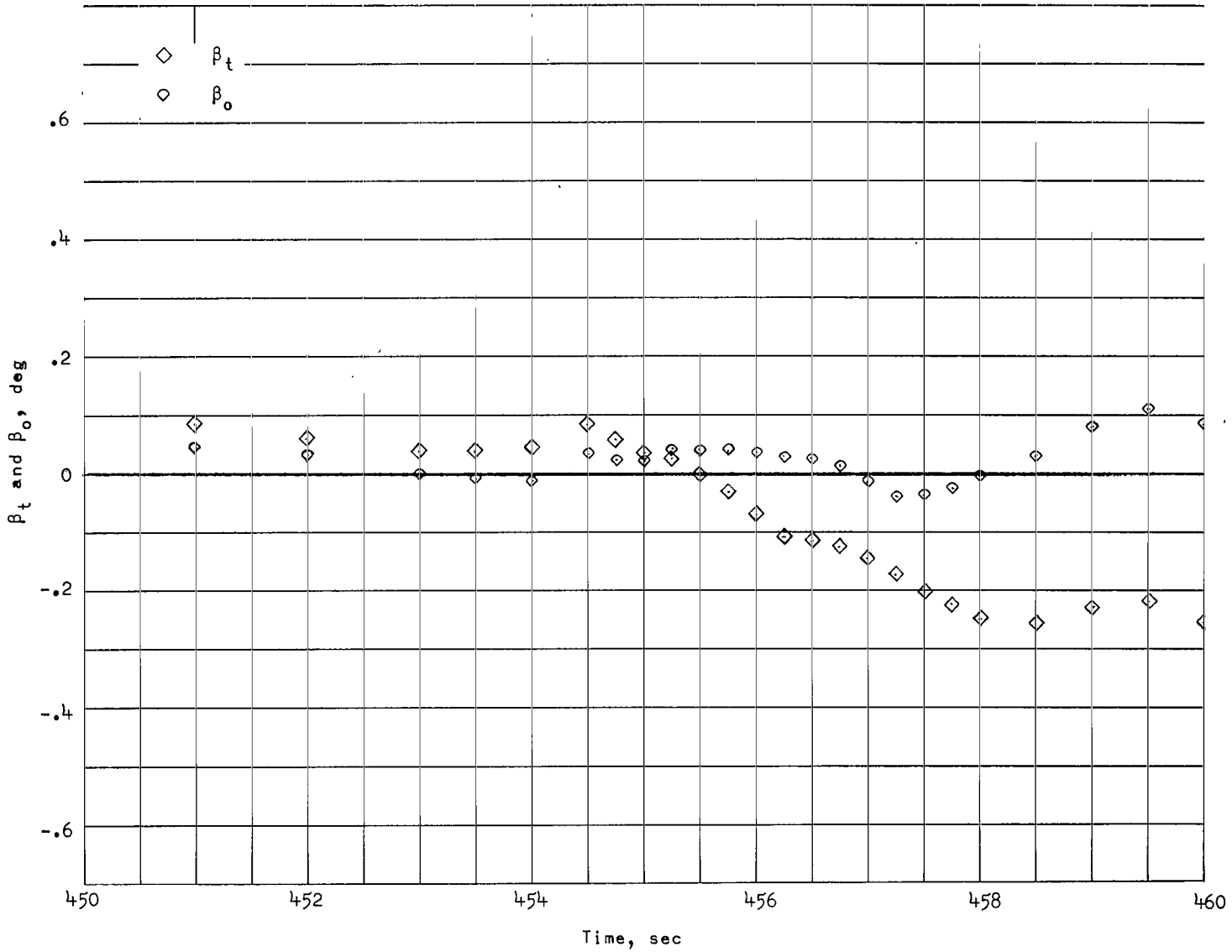

(b) β_t and β_o as a function of time.

Figure 10.- Concluded.

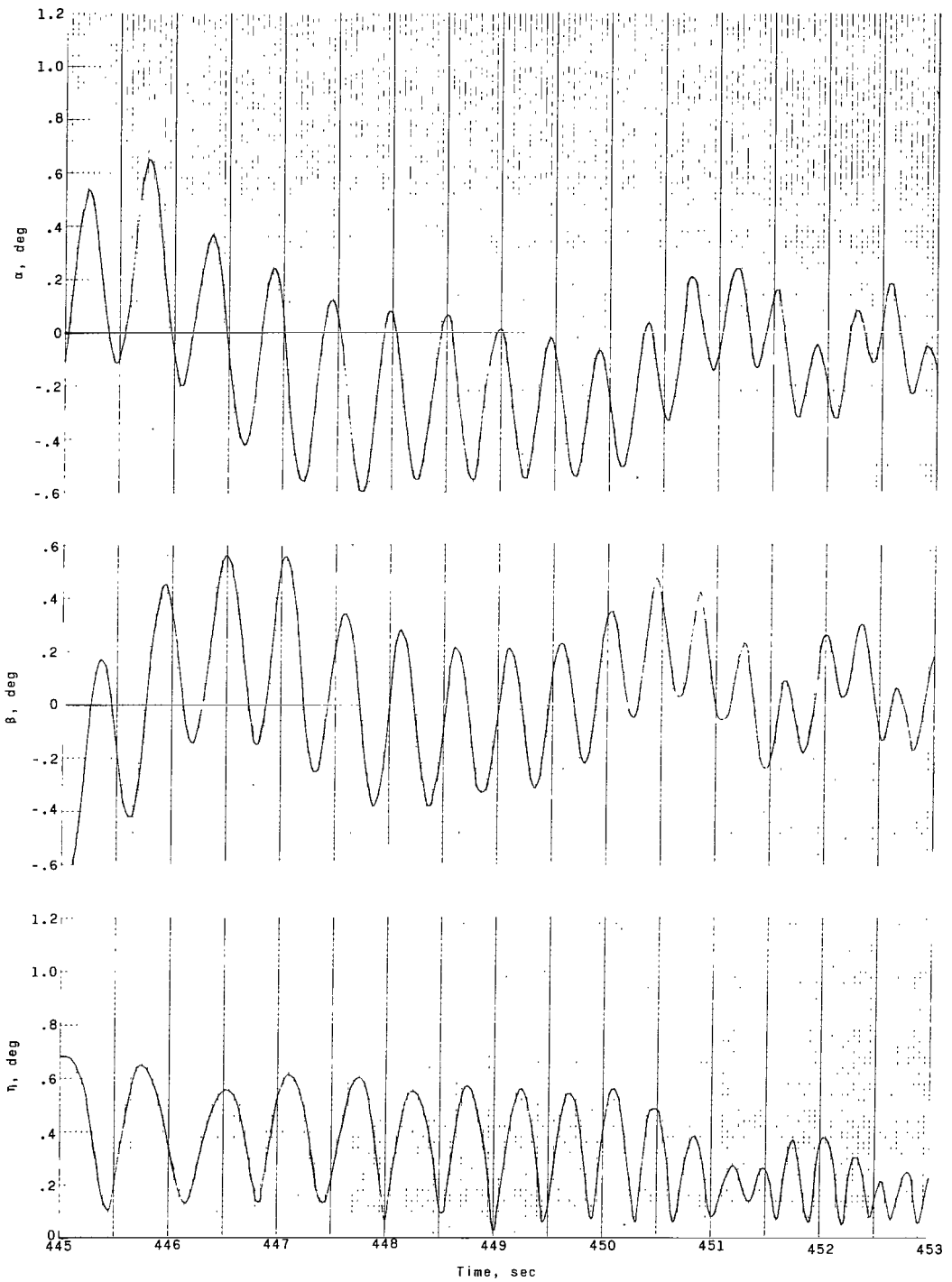

(a) Time = 445 to 453 seconds.

Figure 11.- Angle of attack, angle of sideslip, and total angle of attack as a function of time, determined by a combination force-SLEM method.

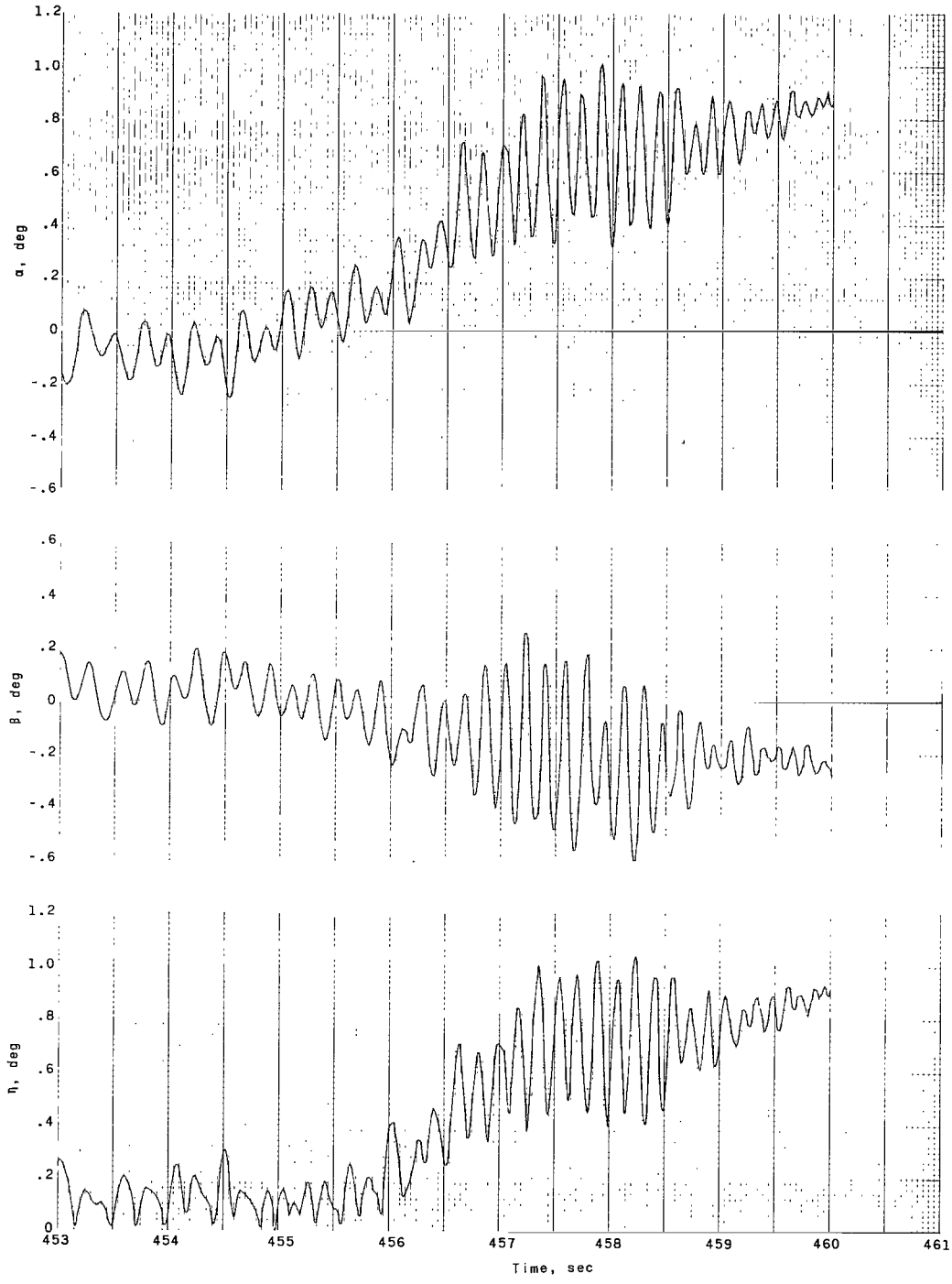

(b) Time = 453 to 461 seconds.

Figure 11.- Concluded.

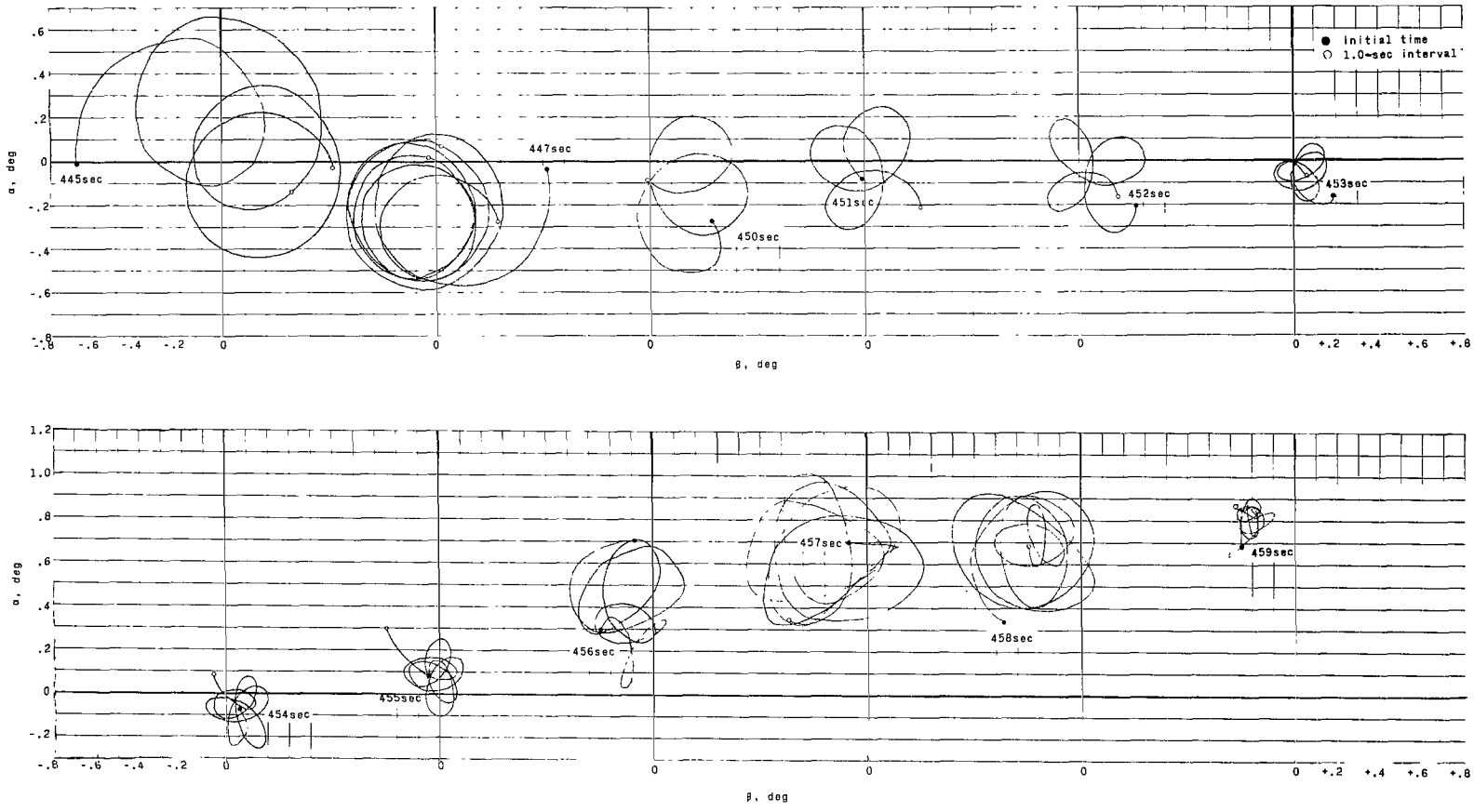

Figure 12.- Crossplot of angle-of-attack and angle-of-sideslip time histories determined by the force-SLEM method.

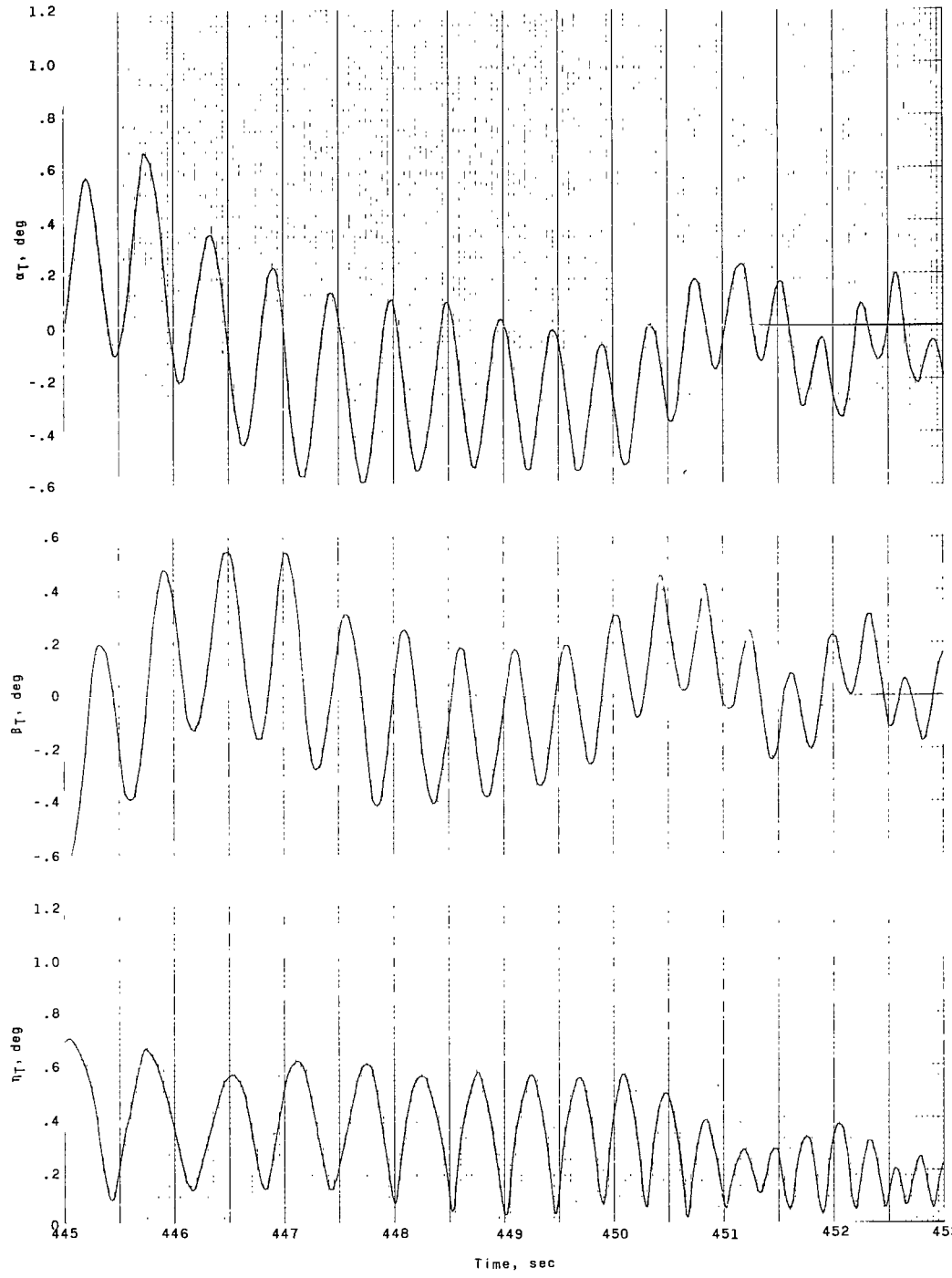

(a) Time = 445 to 453 seconds.

Figure 13.- Angle of attack, angle of sideslip, and total angle of attack as a function of time, determined by the force-SLEM method and rotated into the thermal axis system.

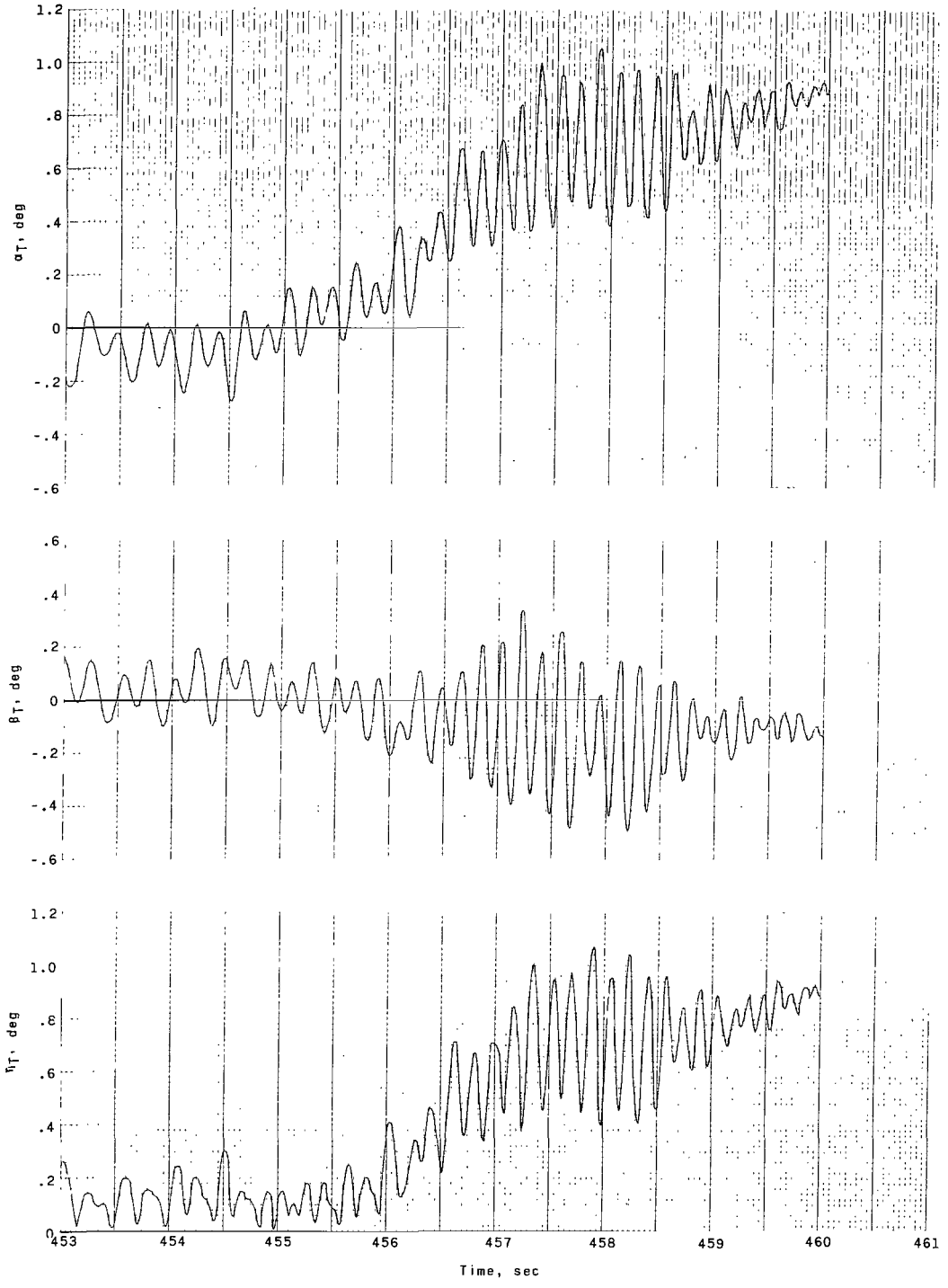

(b) Time = 453 to 461 seconds.

Figure 13.- Concluded.

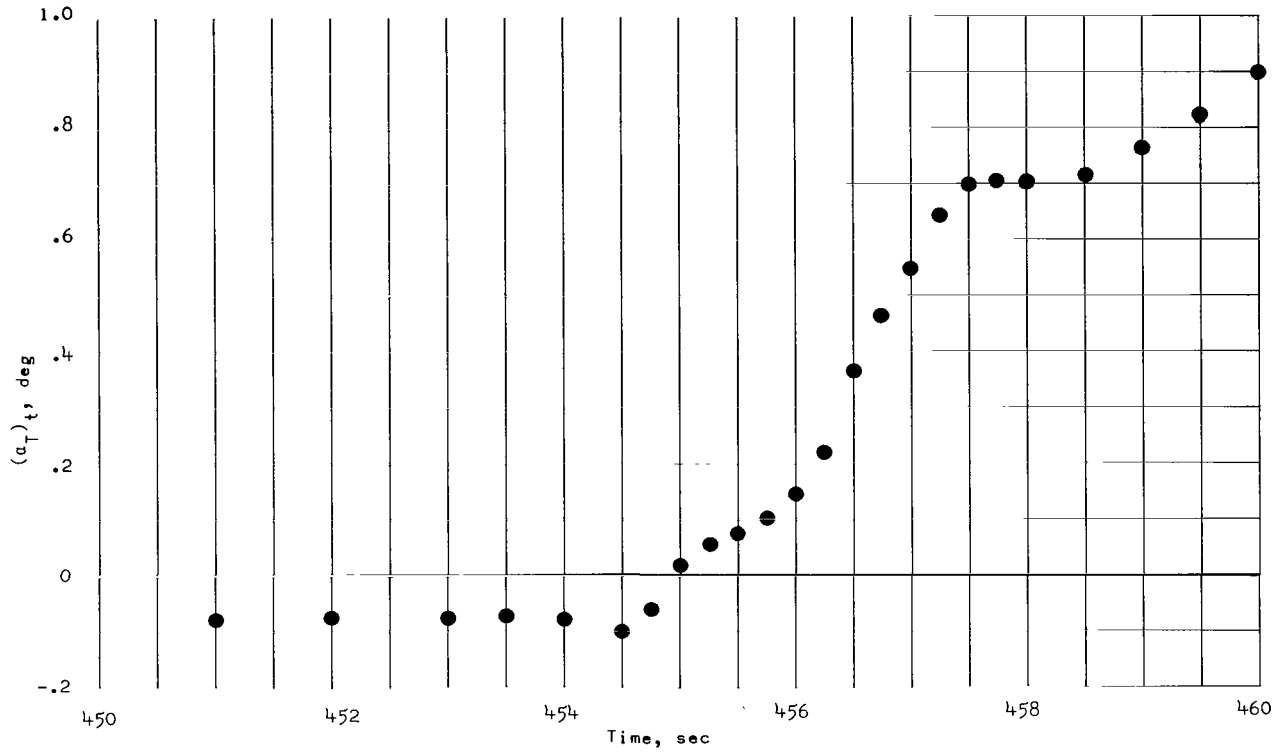

(a) $(\alpha_T)_t$ as a function of time.

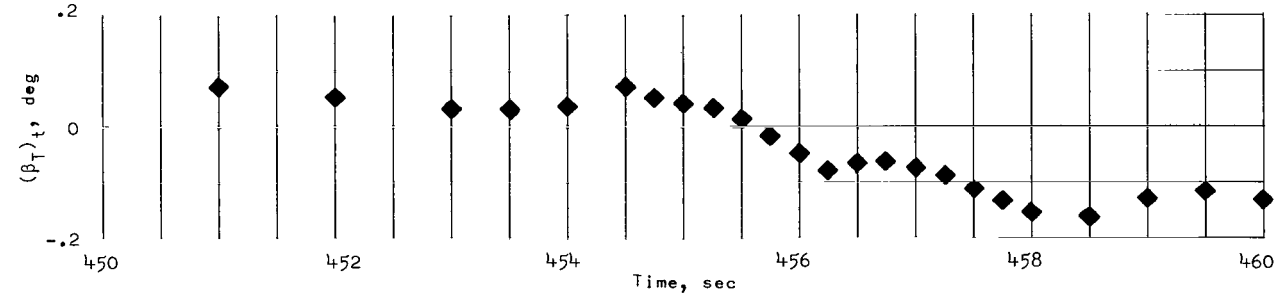

(b) $(\beta_T)_t$ as a function of time.

Figure 14.- Computed trim values in thermal axis system.

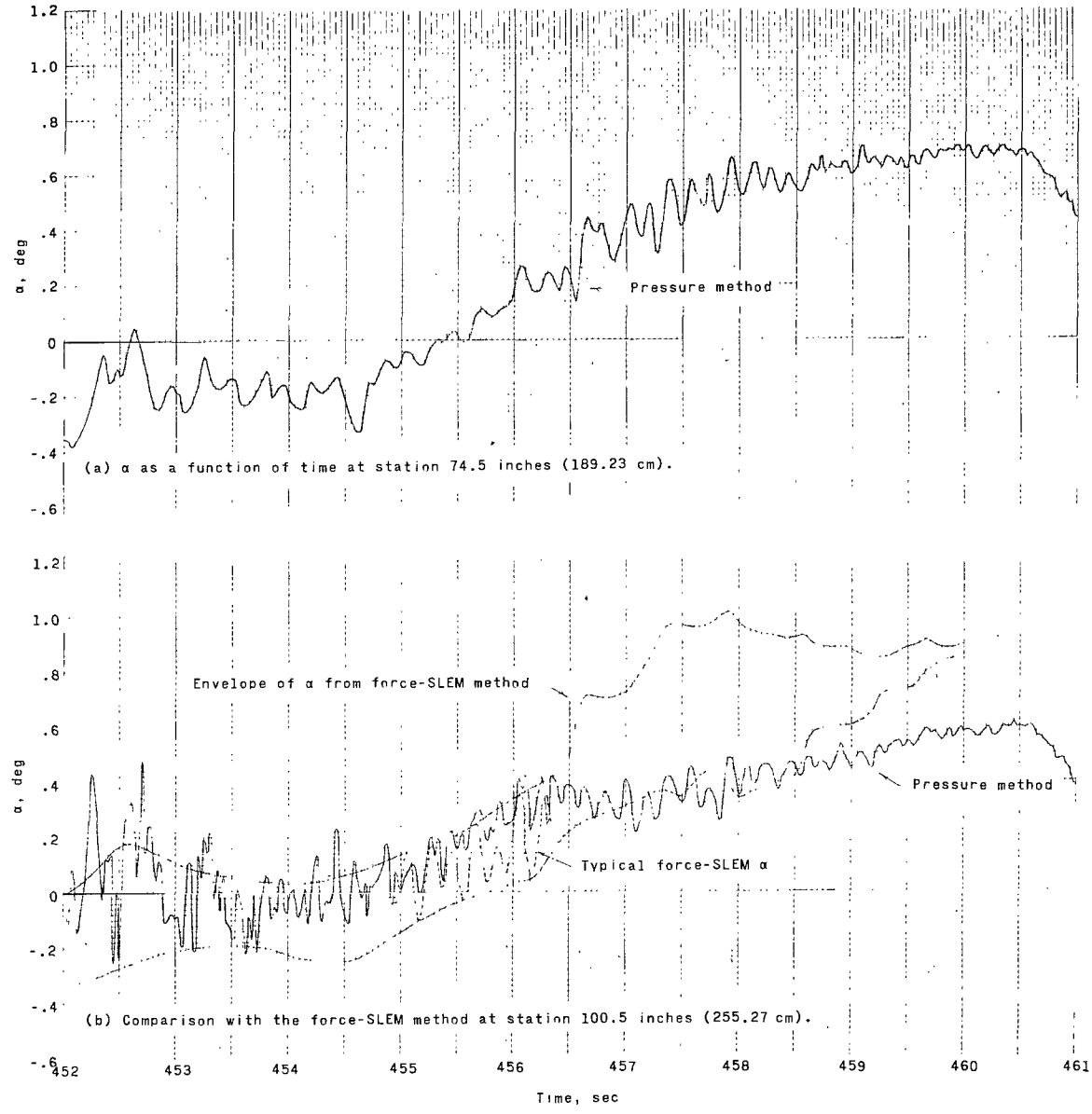

Figure 15.- Angle of attack and angle of sideslip as a function of time, determined by the pressure method.

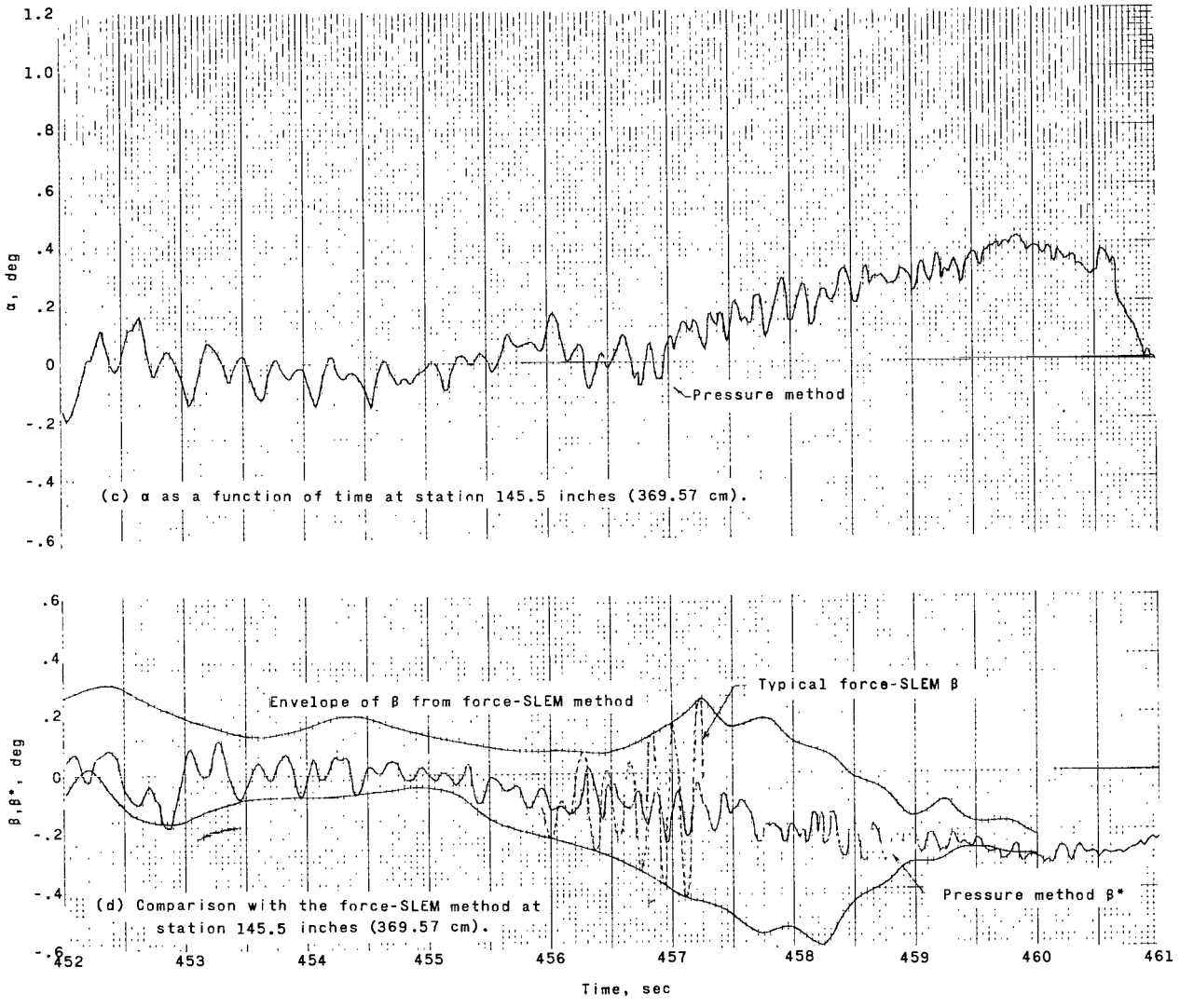

Figure 15.- Concluded.

"The aeronautical and space activities of the United States shall be conducted so as to contribute . . . to the expansion of human knowledge of phenomena in the atmosphere and space. The Administration shall provide for the widest practicable and appropriate dissemination of information concerning its activities and the results thereof."

—NATIONAL AERONAUTICS AND SPACE ACT OF 1958

NASA SCIENTIFIC AND TECHNICAL PUBLICATIONS

TECHNICAL REPORTS: Scientific and technical information considered important, complete, and a lasting contribution to existing knowledge.

TECHNICAL NOTES: Information less broad in scope but nevertheless of importance as a contribution to existing knowledge.

TECHNICAL MEMORANDUMS: Information receiving limited distribution because of preliminary data, security classification, or other reasons.

CONTRACTOR REPORTS: Scientific and technical information generated under a NASA contract or grant and considered an important contribution to existing knowledge.

TECHNICAL TRANSLATIONS: Information published in a foreign language considered to merit NASA distribution in English.

SPECIAL PUBLICATIONS: Information derived from or of value to NASA activities. Publications include conference proceedings, monographs, data compilations, handbooks, sourcebooks, and special bibliographies.

TECHNOLOGY UTILIZATION PUBLICATIONS: Information on technology used by NASA that may be of particular interest in commercial and other non-aerospace applications. Publications include Tech Briefs, Technology Utilization Reports and Notes, and Technology Surveys.

Details on the availability of these publications may be obtained from:

SCIENTIFIC AND TECHNICAL INFORMATION DIVISION

NATIONAL AERONAUTICS AND SPACE ADMINISTRATION

Washington, D.C. 20546